Editors' Suggestion

Photon-recoil and laser-focusing limits to Rydberg gate fidelity

F. Robicheaux,[1,2,3,*] T. M. Graham,[3] and M. Saffman[3,4]

[1]*Department of Physics and Astronomy, Purdue University, West Lafayette, Indiana 47907, USA*
[2]*Purdue Quantum Center, Purdue University, West Lafayette, Indiana 47907, USA*
[3]*Department of Physics, University of Wisconsin-Madison, Madison, Wisconsin 53706, USA*
[4]*ColdQuanta, Inc., 111 N. Fairchild St., Madison, Wisconsin 53703, USA*

(Received 18 November 2020; accepted 3 February 2021; published 24 February 2021)

Limits to Rydberg gate fidelity that arise from the entanglement of internal states of neutral atoms with the motional degrees of freedom due to the momentum kick from photon absorption and re-emission is quantified. This occurs when the atom is in a superposition of internal states but only one of these states is manipulated by visible or UV photons. The Schrödinger equation that describes this situation is presented and two cases are explored. In the first case, the entanglement arises because the spatial wave function shifts due to the separation in time between excitation and stimulated emission. For neutral atoms in a harmonic trap, the decoherence can be expressed within a sudden approximation when the duration of the laser pulses are shorter than the harmonic oscillator period. In this limit, the decoherence is given by simple analytic formulas that account for the momentum of the photon, the temperature of the atoms, the harmonic oscillator frequency, and atomic mass. In the second case, there is a reduction in gate fidelity because the photons causing absorption and stimulated emission are in focused beam modes. This leads to a dependence of the optically induced changes in the internal states on the center of mass atomic position. In the limit where the time between pulses is short, the decoherence can be expressed as a simple analytic formula involving the laser waist, temperature of the atoms, the trap frequency, and the atomic mass. These limits on gate fidelity are studied for the standard π-2π-π Rydberg gate and a protocol based on a single adiabatic pulse with a Gaussian envelope.

DOI: 10.1103/PhysRevA.103.022424

I. INTRODUCTION

Neutral atom qubits with Rydberg state mediated interactions have emerged as a promising platform for scalable quantum computation and simulation [1]. Trap arrays suitable for individual control of 100 and more atomic qubits have been prepared [2–7] and high fidelity one-qubit [8–10] and two-qubit [11–13] gates have been demonstrated. Many protocols have been proposed and analyzed for implementing two-qubit Rydberg gates [12,14–26]. Although detailed analyses accounting for the multilevel atomic structure and finite Rydberg lifetime have identified protocols with the potential of reaching $\mathcal{F} > 0.9999$ [20,27], the studies to date, with the notable exception of Ref. [19], which included a detailed examination of motional errors, have either ignored the limits set by photon recoil or treated it only approximately [14,28,29].

Momentum kicks due to the absorption and emission of photons during a Rydberg pulse, as well as Rydberg-Rydberg interactions, lead to undesired entanglement between qubits encoded in hyperfine states and the atomic center of mass motion. After tracing out the motional state, the remaining entanglement in the qubit basis is reduced, which sets a limit on the gate fidelity [30]. The degree of infidelity depends on several parameters including the magnitude of the photon momentum, the temporal extent of the Rydberg pulse sequence, the initial motional state of the atoms, the characteristic vibrational frequencies of the trap holding the atom, and whether or not the trap is turned off or left on during the Rydberg gate.

In this paper, we present a rigorous analysis of the fidelity limits set by these effects for two representative C_Z gate protocols: the standard π-2π-π pulse sequence [14] and a simple implementation of a C_Z gate that uses only a single Gaussian shaped adiabatic pulse applied simultaneously to both atoms. In both cases, the gate infidelity scales with the change in atomic position x during the gate, relative to the size of the initial center of mass wave function δx. For an atom that is prepared in the motional ground state of the trap, $\delta x \sim 1/\nu^{1/2}$ with ν the trap frequency so the infidelity grows proportional to ν. The scaling of the infidelity follows from the observation that the change in atomic position during the Rydberg gate is fractionally more significant for a well localized spatial wave function, than for a less confined wave function. This counterintuitive result shows that, in contrast to many atomic implementations of quantum protocols, it is not always advantageous to work deep in the Lamb-Dicke limit of tight confinement.

While the analysis that follows is primarily concerned with the infidelity of Rydberg gates we note that single qubit gates between internal states are susceptible to errors analogous to those analyzed here. A prime example of this is given by qubits encoded in ground and metastable, electronically excited states in alkaline earth atoms [31] or trapped ions [32].

The rest of the paper is structured as follows. In Sec. II. we describe the unwanted entanglement that arises between internal and external degrees of freedom due to photon kicks

*robichf@purdue.edu

or Rydberg forces. This is followed in Sec. III with a description of the two gate protocols to be analyzed in detail and a brief recap of the definition of Bell fidelity which we will use to characterize the gate performance. Section IV presents analytical approximations for the infidelity using a Schrödinger equation treatment. Section V presents numerical infidelity results for realistic experimental parameters. The numerical results are based on a full density matrix treatment and are compared with the analytical approximations. The main results are then summarized in a concluding Sec. VI. Additional analysis including different cases of keeping the trapping potential on or off during the gate is provided in appendices.

II. QUBIT DECOHERENCE FROM MOTIONAL STATE ENTANGLEMENT

The quantum state of a trapped atom is described by its motional degrees of freedom as well as quantum numbers characterizing the nuclear and electronic states. Qubits are typically encoded in the electronic degrees of freedom. The most commonly used approach is encoding in hyperfine states of the ground electronic configuration [33], although also metastable electronically excited states may be used. The total state, including all degrees of freedom, can be written as $|\Psi\rangle = |\psi\rangle_{\rm ext} \otimes |\psi\rangle_{\rm int}$ where $|\psi\rangle_{\rm int}$ is the internal state of the atom which is used to encode a qubit and $|\psi\rangle_{\rm ext}$ is the motional state.

Momentum transfer due to photon recoil from absorption and emission induced by the laser pulses that implement gate operations, as well as forces between Rydberg excited atoms, may change the motional state. When changes in the motion are correlated with the internal state the internal and external degrees of freedom can become entangled which, in the context of Rydberg gates, leads to decoherence of the qubit state [33,34]. It is perhaps worth mentioning that in other settings, notably trapped ion quantum computing, controlled entanglement between internal and external degrees of freedom is in fact crucial for gate operation [35].

To see this explicitly consider an initial product of the center of mass motional state and the qubit

$$|\Psi_{\rm i}\rangle = |\psi_{\rm ext}\rangle \otimes (c_0|0\rangle + c_1|1\rangle), \tag{1}$$

where $|c_0|^2 + |c_1|^2 = 1$. After a gate operation this changes to

$$|\Psi_{\rm f}\rangle = c_0\,|\psi_{\rm ext,0}\rangle \otimes |0\rangle + c_1\,|\psi_{\rm ext,1}\rangle \otimes |1\rangle\,. \tag{2}$$

The reduced density operator for the qubit after the gate is

$$\rho = \begin{pmatrix} |c_0|^2 & c_0 c_1^* \chi^* \\ c_0^* c_1 \chi & |c_1|^2 \end{pmatrix},$$

where $\chi = \langle\psi_{\rm ext,0}|\,\psi_{\rm ext,1}\rangle$. Changes in the motional state that are correlated with the qubit state reduce the magnitude of the coherence $|c_0 c_1^* \chi|$. When $|\chi| = 1$ but there is a phase shift it is possible to apply a correcting rotation on the qubit. When $|\chi| < 1$ the error generally cannot be repaired. In the following sections, we will explicitly calculate χ for several possible gate protocols and establish realistic experimental limits on coherence and gate fidelity.

A. Momentum kick for 1 atom

This section discusses how momentum kicks to atoms during gate pulses affect the fidelity of the gate. The most basic example of this situation is a three-state atom in a one dimensional harmonic trap with the absorbed and emitted photons parallel to the allowed motion. In a typical implementation a laser may cause a transition from the qubit state $|1\rangle$ but leave state $|0\rangle$ untouched. We will limit the treatment to the case where the atom is excited from state $|1\rangle$ to Rydberg state $|R\rangle$ and then de-excited as part of the gate. For simplicity, the discussion below is in the wave function picture but all of the results in Sec. V are obtained using density matrices.

A reduction in gate fidelity occurs because the laser pulses create entanglement between the internal states of the atom and its center of mass degrees of freedom, which has been pointed out in several previous works [14,19,28,36]. Consider the case where the atom starts in a separable wave function of the form of Eq. (1). A short laser pulse of duration δt excites state $|1\rangle$ to state $|R\rangle$ and in the process gives the atom a momentum kick $\hbar K$. After a delay τ much shorter than the vibrational period of the atom trap, a second laser pulse in the same direction de-excites state $|R\rangle$ to state $|1\rangle$ giving the atom a momentum kick $-\hbar K$ from the stimulated emission. Although the second momentum kick undoes the change in momentum from the first, the spatial wave function for state $|1\rangle$ will *not* be the same as that for the state $|0\rangle$ because there will be a change in position, $\delta x = \hbar K \tau / M$, and an extra phase accumulation due to the change in kinetic energy during τ. The final wave function can be written as

$$|\Psi_f\rangle = \psi_{f,0}(x) c_0 |0\rangle + c_1[\psi_{f,1}(x)|1\rangle + \psi_{f,R}(x)|R\rangle], \tag{3}$$

where the c_j are as before, the $\psi_{f,0}$ is normalized to one, and the integral of the sum $|\psi_{f,1}|^2 + |\psi_{f,R}|^2$ is normalized to one. Typically, the norm in state $|1\rangle$ is much larger than that in state $|R\rangle$.

The entanglement between the spatial and internal degrees of freedom results in decoherence in the internal states. A measure of the decoherence is

$$\varepsilon = 1 - |\chi|, \tag{4}$$

where

$$\chi = \int_{-\infty}^{\infty} \psi_{f,0}^*(x)\psi_{f,1}(x)dx, \tag{5}$$

which has a magnitude $0 \leqslant |\chi| \leqslant 1$. When $|\chi| = 1$, no entanglement occurred between the spatial and internal states and there is only an overall phase difference between $\psi_{f,0}(x)$ and $\psi_{f,1}(x)$. This is the desired outcome of the gate pulses. There is decoherence for the case $|\chi| < 1$ which can occur even when the norm of $\psi_{f,1}$ is unity because the laser kicks can cause this part of the wave function to evolve into a different region of Hilbert space. From the process described in the previous paragraph, there will be both a magnitude less than one and a complex phase for χ. See the appendices, Sec. D for a derivation of χ for four different excitation styles. We give both the magnitude and phase for χ, but the projection having a norm less than one is more problematic because the change in phase can be compensated for.

B. Momentum transfer for two atoms

Although not due to photon kicks from absorption or emission, there is a source of decoherence due to transient population with double Rydberg character [19]. This entanglement between the internal states of the atom and the atom motion arises because the Rydberg-Rydberg interaction depends on the separation of the atoms leading to an impulse along the line connecting the atoms, but only when the atoms start in the $|11\rangle$ state. We will only consider the case where the duration of the gate pulses is much smaller than the trap period and the atom displacements are small compared to nearest neighbor separations. In this limit, the Rydberg-Rydberg interaction leads to an impulse due to the force between the atoms when they are both excited. This term only enters the $\psi_{f,11}$ part of the wave function and consists of a phase accumulation $\phi = -V_{RR}\tau_{RR}/\hbar$, where

$$\tau_{RR} = \int_{-\infty}^{\infty} P_{RR}(t)dt \tag{6}$$

is effectively the time spent in the double Rydberg state and P_{RR} is the probability both atoms are in the Rydberg state when starting in the $|11\rangle$ state.

Defining the y-direction as pointing from atom 1 to 2, the spatial dependence of the extra phase accumulation can be approximated as $\phi = 6\mathsf{B}(y_2 - y_1)\tau_{RR}/r_{12}$ where the y_j are displacements from the respective trap centers, with r_{12} the distance between the center of the traps, and $\hbar\mathsf{B} = V_{RR}(r_{12})$; this assumes a $1/r_{12}^6$ dependence on the Rydberg-Rydberg interaction and the displacements are small compared to the trap separation. Outside of an overall, irrelevant phase factor, the projection of the $|00\rangle$, $|01\rangle$, or $|10\rangle$ components on that of $|11\rangle$ are the same and is

$$\langle\psi_{f,00}|\psi_{f,11}\rangle = \langle\psi_{f,00}|e^{i\phi}|\psi_{f,00}\rangle \simeq \left\langle 1 + i\phi - \frac{1}{2}\phi^2 \right\rangle$$
$$= 1 - \frac{36\mathsf{B}^2 k_B T_{\rm eff}\tau_{RR}^2}{M\omega_\perp^2 r_{12}^2}, \tag{7}$$

where $\psi_{f,ii'}$ are the spatial components of the wave function Eq. (21), $\omega_\perp$ is the trap frequency in the y direction, and $T_{\rm eff}$ is defined in Eq. (C7). We used the identity $\langle M\omega_\perp^2 y^2\rangle = k_B T_{\rm eff}$ to generalize Eq. (7) to a thermal distribution. For a resonant dipole-dipole interaction $V_{RR}(r_{12}) \propto 1/r_{12}^3$, in which case the 6 in the expression for ϕ changes to 3 and the 36 in Eq. (7) changes to 9.

III. FIDELITY ANALYSIS OF RYDBERG GATES

Our main objective is to understand the effect of photon momentum kicks on the fidelity of Rydberg gate operations. The magnitude of the effect depends on the gate protocol used as well as atomic and laser parameters. By elucidating the role of photon momentum kicks for prototypical examples the trends for other cases may be apparent.

A diagonal phase gate has the general form, apart from an irrelevant global phase, of

$$C_\phi = \mathrm{diag}(1, e^{i\phi_{01}}, e^{i\phi_{10}}, e^{i\phi_{11}}). \tag{8}$$

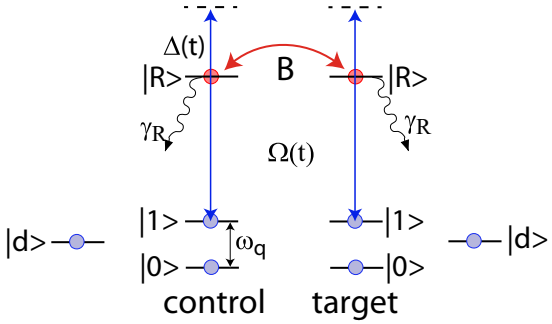

FIG. 1. Energy level structure of neutral atom qubits with ground states $|0\rangle$, $|1\rangle$. Rydberg states $|R\rangle$ interact with strength B. Rydberg states are excited with Rabi frequency $\Omega(t)$ at detuning $\Delta(t)$. Level $|d\rangle$ is an uncoupled state that accumulates spontaneous emission from $|R\rangle$ which has lifetime $\tau_R = 1/\gamma_R$.

The requirement which C_ϕ must satisfy for preparation of fully entangled states is

$$\phi_{01} + \phi_{10} + \phi_{11} = n\pi \tag{9}$$

with n an odd integer. The choice $\phi_{01} = \phi_{10} = \phi_{11} = \pi$ gives a C_Z gate in the standard form of [37]

$$C_Z = \mathrm{diag}(1, -1, -1, -1). \tag{10}$$

Gate protocols that satisfy (9) can be converted into standard form by applying single qubit rotations. We will assume that these can be done perfectly so that any protocol which satisfies (9) will be considered a perfect gate implementation.

A. Rydberg gate protocols

The atomic level structure is shown in Fig. 1. Atoms, each with stable ground states $|0\rangle$, $|1\rangle$, are individually trapped in harmonic potentials. State $|1\rangle$ is optically coupled to Rydberg state $|R\rangle$ while off-resonant excitation of $|0\rangle$ is assumed negligible. The small contribution to gate infidelity from this off-resonant coupling has been considered in Refs. [15,20]. Rydberg excitation is typically implemented as a one- or two-photon process. In the latter case the photons can be sufficiently detuned from an intermediate level that the additional photon scattering is negligible. The two-photon excitation has the advantage that using a counterpropagating geometry the momentum transfer is substantially smaller than for a one-photon implementation.

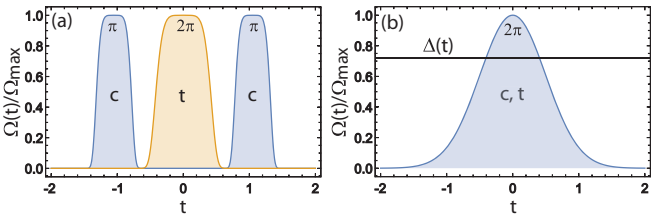

FIG. 2. Rydberg gate protocols. (a) π-2π-π gate [14] with the pulses marked $c(t)$ applied to the control (target) qubits. (b) Adiabatic gate with the same pulse applied to both qubits simultaneously with constant detuning.

The two protocols we analyze in detail are shown in Fig. 2. The first is the π-2π-π protocol, the fidelity of which using constant amplitude pulses has been analyzed in detail in [15]. Neglecting the motional effects considered here, the gate fidelity is limited by atomic structure parameters to less than $\mathcal{F} \sim 0.998$. Higher fidelity reaching $\mathcal{F} > 0.9999$ can be achieved using shaped pulses [20]. The gap between the control atom π pulses plays a dominant role in the sensitivity of this protocol to motional decoherence [29].

The second protocol we consider consists of a single adiabatic pulse applied simultaneously to both atoms with a Gaussian amplitude profile and constant detuning as shown in Fig. 2(b). This gate is similar in concept to the Rydberg dressing gate [19], and other adiabatic gate protocols [25,26], but has a simplified implementation requiring only a single pulse with a constant laser detuning.

The entanglement mechanism of a single adiabatic pulse can be understood from analysis of the coherent part of the atomic dynamics depicted in Fig. 1. Consider first the simplified one-atom problem described by

$$\hat{H}_1 = \hbar \begin{pmatrix} 0 & \Omega^*/2 \\ \Omega/2 & -\Delta \end{pmatrix}$$

in the basis $(|1\rangle, |R\rangle)$. Here we have ignored the far detuned coupling of $|0\rangle$ to the Rydberg state. $\hat{H}_1$ has eigenvalues $\hbar\lambda_{1,2} = \hbar(-\Delta \pm \sqrt{\Delta^2 + |\Omega|^2})/2$ and eigenvectors $\mathbf{u}_{1,2}$. At the beginning of the Gaussian pulse $\Omega(0) = 0$ and the state is $|\psi\rangle = |1\rangle = \binom{1}{0} = \mathbf{u}_1$. As long as the evolution is adiabatic $|\psi(t)\rangle = \mathbf{u}_1$ at all times so the atom returns to the ground state independent of the length of the pulse. This imparts robustness with respect to the amplitude of $\Omega(t)$.

The adiabatic condition is $|\frac{d\theta}{dt}| \ll |\lambda_2 - \lambda_1| = \sqrt{\Delta^2 + |\Omega|^2}$ with θ the mixing angle. The dynamical phase acquired by the state during an adiabatic pulse of duration T is $\phi_{01} = \phi_{10} = \int_0^T dt\, \lambda_1(t) = \int_0^T dt\, (\Delta(t) + \sqrt{\Delta^2(t) + |\Omega(t)|^2})/2$. Setting Δ constant and $\Omega(t) = \Omega_{\max}(e^{-(t-T/2)^2/\sigma^2} - e^{-T^2/4\sigma^2})/(1 - e^{-T^2/4\sigma^2})$ the phase can be found numerically as a function of Δ, $\Omega_{\max}$, and σ.

When the qubits are symmetrically excited the Hamiltonian in the two-atom symmetric basis $(|11\rangle, \frac{|1R\rangle + |R1\rangle}{\sqrt{2}}, |RR\rangle)$ is

$$\hat{H}_2 = \hbar \begin{pmatrix} 0 & \Omega^*/\sqrt{2} & 0 \\ \Omega/\sqrt{2} & -\Delta & \Omega^*/\sqrt{2} \\ 0 & \Omega/\sqrt{2} & -2\Delta + \mathsf{B} \end{pmatrix}.$$

Here Ω is the one atom Rabi frequency coupling states $|1\rangle$ and $|R\rangle$. Diagonalizing $\hat{H}_2$ we obtain eigenvalues $\hbar\lambda_{1,2,3}$ and eigenvectors $\mathbf{u}_{1,2,3}$. Explicit expressions for the eigenvalues are given in [1]. As for the case of a single Rydberg coupled atom the dynamical phase ϕ_{11} is found from integrating the relevant eigenvalue over the duration of the pulse. The result depends on $\Delta, \Omega_{\max}, \sigma$, and B. For any value of B, which is fixed by the choice of Rydberg states and the interatomic spacing $\mathbf{r}_{12}$, we have two free parameters $\Delta/\Omega_{\max}$ and σ, which can be chosen to satisfy the condition on the phases for an entangling C_Z gate.

Examples of valid gate parameters for different interaction strengths are given in Sec. V B. As we will show the adiabatic gate can achieve high fidelity for a wide range of interaction strengths including the limit of strong blockade when $|\mathsf{B}| \gg \Omega_{\max}$ as well as the opposite limit of $|\mathsf{B}| \ll \Omega_{\max}$. In the latter case the doubly excited state $|RR\rangle$ is populated which leads to additional motional errors from Rydberg-Rydberg forces.

B. Bell state fidelity

We will quantify the fidelity of the C_Z gate by calculating the fidelity of the Bell state $|B\rangle = (|00\rangle + |11\rangle)/\sqrt{2}$ which can be prepared by a perfect gate operation. The sequence starts with the separable state $|11\rangle$. Applying the Hadamard gate to both qubits gives

$$|\text{in}\rangle \equiv \mathsf{H}_1\mathsf{H}_2|11\rangle = \tfrac{1}{2}(|00\rangle - |01\rangle - |10\rangle + |11\rangle). \quad (11)$$

Applying the Rydberg C_Z gate (defined to be $\text{diag}(C_Z) = [1, -1, -1, -1]$) followed by a Hadamard gate on qubit 2 gives the Bell state, $|B\rangle$ under perfect operation. In what follows, we will evaluate the implementation of the C_Z gate by starting in a separable density matrix

$$\hat{\rho}_i = |\text{in}\rangle\langle\text{in}|\rho_s(\mathbf{r}_1, \mathbf{r}_2; \mathbf{r}_1', \mathbf{r}_2') \quad (12)$$

where the ρ_s contains the spatial information about the two atom system and could be an eigenstate or a thermal state of the two atoms. We will then solve the density matrix equation for the C_Z gate

$$\frac{d\hat{\rho}(t)}{dt} = \frac{1}{i\hbar}[\hat{H}(t), \hat{\rho}(t)] + \hat{\mathcal{L}}(\hat{\rho}), \quad (13)$$

where $\hat{H}(t)$ is the time-dependent Hamiltonian which will include the kick from photon absorption or emission. In the calculations, we will simulate the case where the qubit $|1\rangle$ can be excited to a Rydberg state $|R\rangle$. For the two-atom Hamiltonian, we use $\hat{H} = \hat{H}_1 \otimes \hat{I} + \hat{I} \otimes \hat{H}_1 + \hat{H}_2$ where $\hat{H}_1$ is a one-atom operator and $\hat{H}_2$ describes the Rydberg interaction.

As a basic example, plane wave light propagating in the x direction will give a one atom Hamiltonian

$$\hat{H}_1 = H_C - \hbar\Delta|R\rangle\langle R| + \frac{\hbar\Omega}{2}(e^{iKx}|R\rangle\langle 1| + e^{-iKx}|1\rangle\langle R|), \quad (14)$$

where H_C represents the kinetic energy and confining potential for each atom, Δ is the detuning of the laser connecting states $|1\rangle$ and $|R\rangle$, K is the photon wave number, and Ω is the Rabi frequency. In addition to the one atom Hamiltonian, there is a Rydberg-Rydberg interaction

$$\hat{H}_2 = \hbar\mathsf{B}|RR\rangle\langle RR|, \quad (15)$$

where $\hbar\mathsf{B}$ is the energy shift of the pair Rydberg state. The Rydberg state can decay by spontaneous photon emission or by absorption or emission of black-body photons. If the Rydberg state decays, the time to return to the ground state manifold can be large compared to the gate duration and there are many more hyperfine ground states than the qubit pair. Thus we will use the pessimistic approximation that all of the radiative loss goes to states outside of the qubit pair or the Rydberg state. This population can be assigned to the single

dark state $|d\rangle$ giving

$$\hat{\mathcal{L}}(\hat{\rho}) = \Gamma \sum_{j=1}^{2} \left(|d\rangle\langle R_j|\hat{\rho}|R_j\rangle\langle d| - \frac{1}{2}|R_j\rangle\langle R_j|\hat{\rho} - \frac{1}{2}\hat{\rho}|R_j\rangle\langle R_j| \right), \tag{16}$$

where j labels the two atoms.

Various gate protocols have different time dependence in the coupling $\Omega(t)$, and the detuning $\Delta(t)$. In some cases, the confining potential $H_{C,j}$ can depend on time and on the internal state of the atom.

In practice, we solve the density matrix equations using a basis set of harmonic oscillator states at angular frequency ω for the center of mass motion; in cases where more than 1D motion is important, we will distinguish between angular frequencies of the center of mass motion parallel, $\omega_\parallel$, or perpendicular, $\omega_\perp$, to the beam propagation direction. This gives

$$\hat{\rho} = \sum |i_1 i_2\rangle\langle i_1' i_2'| \psi_{v_1}(\mathbf{r}_1)\psi_{v_2}(\mathbf{r}_2)\psi^*_{v_1'}(\mathbf{r}_1')\psi^*_{v_2'}(\mathbf{r}_2') \times \rho_{i_1 v_1 i_2 v_2 i_1' v_1' i_2' v_2'}, \tag{17}$$

where $|i\rangle$ are the internal states $|0\rangle$, $|1\rangle$, $|R\rangle$, or $|d\rangle$ and the v indicate the vibrational quantum numbers where each v_j could be 1, 2, or 3 indices depending on the spatial dimension of the simulation. The number of vibrational states needed for convergence depends on the temperature in the simulation [more states are needed as $k_B T/(\hbar\omega)$ increases] and the photon momentum (more states are needed as K increases).

The reduced density matrix is defined as

$$\rho_{i_1 i_2 i_1' i_2'} = \sum_{v_1 v_2} \rho_{i_1 v_1 i_2 v_2 i_1' v_1 i_2' v_2} \tag{18}$$

where we will not use a special symbol for the reduced density matrix since it has four indices instead of the eight for the full density matrix. The reduced density matrix is used in the calculation of the gate fidelity.

After solving the time dependent density matrix equation, Eq. (13), for the C_Z gate, we add a phase to state $|1\rangle$ and then apply a Hadamard gate to qubit 2. The phase is chosen to maximize the Bell state fidelity. High fidelity single qubit gate operations have been demonstrated on atomic qubits [8,10] and it is possible to use magic trapping techniques so the center of mass vibrational frequencies are identical for both qubit states [38,39]. We therefore assume the phase on state $|1\rangle$ and the Hadamard gate can be perfectly implemented irrespective of the vibrational state. The Bell state fidelity is defined as [40]

$$\mathcal{F} = \frac{\rho_{0000} + \rho_{1111}}{2} + |\rho_{0011}| \leqslant 1. \tag{19}$$

The C_Z gate protocol is designed to make $\mathcal{F}$ as large as possible. The requirement for scalable quantum computation depends on the error correction scheme [41], but $\mathcal{F} > 0.99$ is generally considered a minimum fidelity below which very large numbers of qubits are required.

To simplify many of the derivations, we will use a wave function picture to track the effects from a gate although all of the results are ultimately derived from the density matrix in Eq. (19). The initial state can be written as

$$|\Psi_i\rangle = |\text{in}\rangle\psi_i(\mathbf{r}_1, \mathbf{r}_2), \tag{20}$$

where $|\text{in}\rangle$ is defined in Eq. (11). A gate will cause a manipulation of the spatial part of the wave function depending on the internal state. Ignoring the part of the wave function left in the states outside of the qubit pair, the wave function after the gate has the form

$$|\Psi_f\rangle = \tfrac{1}{2}(|00\rangle\psi_{f,00} + |01\rangle\psi_{f,01} + |10\rangle\psi_{f,10} - |11\rangle\psi_{f,11}) \tag{21}$$

where the $\psi_{f,ii'}$ have the effects of different interactions between the atoms and have norm $\sim$1.

Applying the Hadamard gate to qubit 2 gives the final state

$$|\Psi\rangle = \frac{1}{\sqrt{2}}\left(|00\rangle\frac{\psi_{f,00}+\psi_{f,01}}{2} + |11\rangle\frac{\psi_{f,11}+\psi_{f,10}}{2} + |01\rangle\frac{\psi_{f,00}-\psi_{f,11}}{2} + |10\rangle\frac{-\psi_{f,11}+\psi_{f,10}}{2} \right). \tag{22}$$

From this, taking $|\Psi\rangle\langle\Psi|$ and integrating over the spatial coordinates gives the components of the reduced density matrix

$$\begin{aligned} \rho_{0000} &= \tfrac{1}{8}(\langle\psi_{f,00}| + \langle\psi_{f,01}|)(|\psi_{f,00}\rangle + |\psi_{f,01}\rangle), \\ \rho_{1111} &= \tfrac{1}{8}(\langle\psi_{f,11}| + \langle\psi_{f,10}|)(|\psi_{f,11}\rangle + |\psi_{f,10}\rangle), \\ \rho_{0011} &= \tfrac{1}{8}(\langle\psi_{f,00}| + \langle\psi_{f,01}|)(|\psi_{f,11}\rangle + |\psi_{f,10}\rangle). \end{aligned} \tag{23}$$

IV. ANALYTICAL ESTIMATES OF MOTIONAL GATE INFIDELITY

This section provides an analytical treatment of two different gate protocols to give an idea of the parameters that determine the contribution of photon momentum to the gate infidelity, $1 - \mathcal{F}$. This derivation often will be based on the Schrödinger equation since the other effects are small. We will then average over possible spatial states to account for cases where the atom is not in a motional eigenstate. These analytical results are used for interpretation; for the example results below, we always solve the density matrix equations, Eq. (13).

A. Bell fidelity for π-2π-π C_Z gate

To see how entanglement between the internal qubit state and the atomic center of mass motion affects the Bell fidelity, the π-2π-π Rydberg blockade gate is instructive. In this case, a first pulse excites qubit 1 to the Rydberg state if it is in state $|1\rangle$, a second pulse excites qubit 2 from state $|1\rangle$ to the Rydberg state and back to state $|1\rangle$ if qubit 1 is *not* in the Rydberg state, and a last pulse de-excites qubit 1 from the Rydberg state back to $|1\rangle$. We will consider three contributions to infidelity: axial momentum kicks, laser focusing, and radiative losses.

Contribution from axial momentum

To derive the effect from axial momentum, the effects on the $\psi_{f,ii'}$ from the different kicks must be determined. The $\psi_{f,00}$ has no kick from momentum absorption, the $\psi_{f,10}$ has a kick on qubit 1 and no kick on qubit 2, the $\psi_{f,01}$ has a kick on qubit 2 and no kick on qubit 1, and $\psi_{f,11}$ has the same kick on qubit 1 as for $\psi_{f,10}$. All of the far off resonant qubit transitions get a small kick from off resonant Stark shifts (for example, qubit 1 in $\psi_{f,00}$ and qubit 2 in $\psi_{f,11}$). The effect of

the kick on qubit 1 can be approximated using the results in Sec. D 2 while that on qubit 2 for $\psi_{f,01}$ can be approximated using the results in Sec. D 1. The kicks from off resonant shifts can be calculated using the results in Sec. D 3. Even when the excitation to the Rydberg state is through a nearly resonant 2 photon transition, the population out of the ground state is small and each pulse length is small compared to the duration of the gate. This means the kicks from off resonant shifts can be ignored compared to the momentum kicks.

We will write the unkicked wave function as ψ_0 and the kicked wave function as $\psi_{k,1}$ for the kick on atom 1 and $\psi_{k,2}$ for the kick on atom 2. From the previous paragraph, the different wave functions can be written as

$$\begin{aligned}\psi_{f,00} &= \psi_0(\mathbf{r}_1)\psi_0(\mathbf{r}_2),\\ \psi_{f,01} &= \psi_0(\mathbf{r}_1)\psi_{k,2}(\mathbf{r}_2),\\ \psi_{f,10} &= \psi_{k,1}(\mathbf{r}_1)\psi_0(\mathbf{r}_2),\\ \psi_{f,11} &= \psi_{k,1}(\mathbf{r}_1)\psi_0(\mathbf{r}_2).\end{aligned} \tag{24}$$

The projections needed to determine the fidelity are

$$1 - |\langle\psi_{k,i}|\psi_0\rangle| = \varepsilon^{(i)} \tag{25}$$

with $\varepsilon^{(1)}$ from Sec. D 2, Eq. (D11), while $\varepsilon^{(2)}$ is derived in Sec. D 1, Eq. (D5).

We use these terms in the wave function in Eq. (23) to find

$$\begin{aligned}\rho_{0000} &= \tfrac{1}{4}(2-\varepsilon^{(2)}),\\ \rho_{1111} &= \tfrac{1}{2},\\ \rho_{0011} &= \tfrac{1}{4}(1-\varepsilon^{(1)})(2+\varepsilon^{(2)}).\end{aligned} \tag{26}$$

These expressions do not include phase corrections from the momentum kicks and far off resonant Stark shifts mentioned above. These phases can be corrected by single qubit Z rotations in order to recover an ideal C_Z gate, and are therefore not retained in the analysis. Putting in the analytic forms for the ε and dropping terms of order ε^2, the Bell infidelity is

$$1-\mathcal{F} = \frac{\varepsilon^{(1)}}{2} + \frac{3\varepsilon^{(2)}}{8} = \frac{K^2 k_B T_{\text{eff}}}{2M}\left(\frac{\tau_1^2}{2} + \frac{3\tau_2^2}{8}\right), \tag{27}$$

where T_{eff} is from Eq. (C7), τ_1 is the time between the two π pulses, and $\tau_2 = \delta t/2$ with δt the duration of the 2π pulse. The time between π pulses is several times larger than the duration of the 2π pulse which suggests $\varepsilon^{(1)} \gg \varepsilon^{(2)}$. When the temperature is much larger than the quantized energy spacings of the atom trap, $T_{\text{eff}} \simeq T$ and Eq. (27) is identical to the "Doppler dephasing" term in Ref. [11] Supplementary Material, which differs by a factor of 2 from that in Ref. [29].

B. Contribution from laser focusing

The finite spatial extent of an atom's position combined with spatial variation of the laser intensity due to focusing leads to infidelity in the gate. In this section, we will only treat this effect. There are several trends to consider. As the laser waist decreases, the spatial variation of the intensity increases across the spatial extent of the atom position leading to decreased fidelity. The fidelity decreases with increasing temperature due to the increasing spatial extent. The fidelity increases as the trap frequency increases due to the decreasing spatial extent.

To obtain the infidelity due to laser focusing, the projection derived in Sec. F will be used. The decreased norm in each term can be found by noting that in $\psi_{f,00}$ neither atom is excited, $\psi_{f,10}$ atom 1 is excited, $\psi_{f,01}$ atom 2 is excited, and $\psi_{f,11}$ has no effect since the 2π pulse changes the sign of the ψ_{11} term *not* excited to ψ_{R1} in the first π pulse. Unlike the previous section, the main effect is the change in the norm of the state associated with the transition to the Rydberg state and back. In this case, the different wave functions can be written as

$$\begin{aligned}\psi_{f,00} &= \psi_{i,00},\\ \psi_{f,01} &= (1-\varepsilon^{(G)})\psi_{i,00},\\ \psi_{f,10} &= (1-\varepsilon^{(G)})\psi_{i,00},\\ \psi_{f,11} &= \psi_{i,00}.\end{aligned} \tag{28}$$

Substituting the projections into Eq. (23), gives

$$\rho_{0000} = \rho_{1111} = |\rho_{0011}| = \frac{1}{2} - \frac{\varepsilon^{(G)}}{2} + \frac{(\varepsilon^{(G)})^2}{8}, \tag{29}$$

where $\varepsilon^{(G)}$ is defined in Eq. (F5). Dropping all terms involving ε^2 the Bell state fidelity, Eq. (19), gives

$$1-\mathcal{F} = \varepsilon^{(G)}. \tag{30}$$

If the excitation is due to two photon absorption, the $1/w_0^2$ is the sum of the squares of the inverse waists and the $1/x_R^2$ is the sum of the squares of the inverse Rayleigh ranges.

C. Contribution from radiative losses

The contribution to the infidelity due to radiative losses can be computed from the form of Eq. (23) by considering the decrease in magnitude in each part of the wave function. We will take the most pessimistic interpretation that radiative losses due to spontaneous emission or blackbody radiation lead to transitions outside of the qubit states on the time scale relevant to the gate. Assuming the Rydberg lifetime is much shorter than the gate duration, the change in norm leads to

$$\begin{aligned}\psi_{f,00} &= \psi_{i,00},\\ \psi_{f,01} &= \left(1-\frac{\Gamma\tau_2}{2}\right)\psi_{i,00},\\ \psi_{f,10} &= \left(1-\frac{\Gamma\tau_1}{2}\right)\psi_{i,00},\\ \psi_{f,11} &= \left(1-\frac{\Gamma\tau_1}{2}\right)\psi_{i,00}.\end{aligned} \tag{31}$$

Using Eqs. (23) and (19) and dropping terms quadratic in τ leads to the infidelity

$$1-\mathcal{F} = \Gamma\left(\frac{\tau_1}{2} + \frac{\tau_2}{4}\right), \tag{32}$$

where Γ is the inverse of the Rydberg lifetime due to radiative losses, τ_1 is the time between the two π pulses, and $\tau_2 = \delta t/2$ with δt the duration of the 2π pulse.

D. Bell fidelity for adiabatic C_Z gate

Another possible gate protocol involves exciting both qubits simultaneously with the same laser pulse. We will

let $\Omega(t)$ have a Gaussian envelope with fixed detuning Δ. This will give a C_Z if the detuning, duration, and Rydberg-Rydberg interaction, $\hbar\mathsf{B}$, are chosen appropriately. The one atom Hamiltonian is Eq. (14) with

$$\Omega(t) = \Omega_0 e^{-t^2/\delta t^2} \tag{33}$$

the only time dependent part.

As in the previous section, the final wave function has the form of Eq. (21) where the $\psi_{f,ii'}$ have the effects of different kicks. The $\psi_{f,00}$ has no kick from the photon momentum, the $\psi_{f,10}$ has a kick on qubit 1 and no kick on qubit 2, the $\psi_{f,01}$ has the same kick on qubit 2 and no kick on qubit 1, and the $\psi_{f,11}$ has a kick on both qubits. There are small kicks from far detuned transitions which will be ignored. The results from Sec. D 3 can be used to compute the effect on $\psi_{f,10}$ and $\psi_{f,01}$. The effect on $\psi_{f,11}$ is more difficult to obtain because it involves both qubits.

Because there are four electronic states involved and two different atomic momenta, we were not able to derive an expression for the projections involving $\psi_{f,11}$. However, we have found a formula using qualitative arguments that gives good agreement with all of the calculations we have performed with the full density matrix. The idea is to treat the adiabatic pulse on the $\psi_{f,11}$ state as giving the same kick to each atom. In analogy to Eq. (D16), we define the duration of the kick on an individual atom as half of the Rydberg population integrated over the pulse:

$$\tau_R = \frac{1}{2}\int_{-\infty}^{\infty} P_{R1}(t) + P_{1R}(t) + 2P_{RR}(t)dt, \tag{34}$$

where $P_{R1}(t)$ is the probability for atom 1 to be in the Rydberg state and atom 2 is in state $|1\rangle$, $P_{1R}(t)$ is the reverse identification, and $P_{RR}(t)$ is the probability that both atoms are in the Rydberg state. For the symmetric excitation of this gate, $P_{R1}(t) = P_{1R}(t)$. This calculation requires hardly any computer time compared to solving the full density matrix equations including the vibrational states. This leads to the identification

$$\begin{aligned}
\psi_{f,00} &= \psi_0(\mathbf{r}_1)\psi_0(\mathbf{r}_2),\\
\psi_{f,01} &= \psi_0(\mathbf{r}_1)\psi_{k,1}(\mathbf{r}_2),\\
\psi_{f,10} &= \psi_{k,1}(\mathbf{r}_1)\psi_0(\mathbf{r}_2),\\
\psi_{f,11} &= \psi_{k,2}(\mathbf{r}_1)\psi_{k,2}(\mathbf{r}_2)
\end{aligned} \tag{35}$$

with the projections from Eq. (D17)

$$\begin{aligned}
1 - |\langle\psi_0|\psi_{k,1}\rangle| &= \varepsilon^{(ad)}(\tau_a),\\
1 - |\langle\psi_0|\psi_{k,2}\rangle| &= \varepsilon^{(ad)}(\tau_R),\\
1 - |\langle\psi_{k,1}|\psi_{k,2}\rangle| &= \varepsilon^{(ad)}(\tau_R - \tau_a),
\end{aligned} \tag{36}$$

where τ_a is from Eq. (D16) and τ_R is from Eq. (34).

Ignoring all terms quadratic in the ε, the projections in Eq. (23) give

$$\begin{aligned}
\rho_{0000} &= \frac{1}{2} - \frac{K^2 k_B T_{\rm eff}}{2M}\frac{\tau_a^2}{4},\\
\rho_{1111} &= \frac{1}{2} - \frac{K^2 k_B T_{\rm eff}}{2M}\frac{\tau_R^2 + (\tau_R - \tau_a)^2}{4},\\
|\rho_{0011}| &= \frac{1}{2} - \frac{K^2 k_B T_{\rm eff}}{2M}\frac{3\tau_R^2 + 3\tau_a^2 + (\tau_R - \tau_a)^2}{8},
\end{aligned} \tag{37}$$

where τ_a is from Eq. (D16) and τ_R is from Eq. (34). Both of these times are computed using only the internal states of the atoms. Combining these factors, the Bell state infidelity due to the photon momentum kicks is

$$1 - \mathcal{F} = \frac{K^2 k_B T_{\rm eff}}{2M}\left(\frac{\tau_a^2}{2} + \frac{\tau_R^2}{2} + \frac{(\tau_R - \tau_a)^2}{4}\right), \tag{38}$$

which can be compared to the same expression for the π-2π-π gate of the previous section, Eq. (27). Although the details are different, the gates have the same scaling with photon kick $\hbar K$, atom mass M, and effective temperature $T_{\rm eff}$. An advantage of the adiabatic gate is that the time spent in the Rydberg state, as measured by τ_a and τ_R, can be substantially shorter than the spacing of the π pulses τ_1 in the π-2π-π gate for the same excitation Rabi frequency. This gate also has the advantage that it can reach high fidelity for both large and small B, the latter case being useful for gates acting on qubits with large spatial separations.

In addition to the axial momentum kick, the Rydberg lifetime and the laser focus will contribute to infidelity. It is not obvious how to analytically account for these effects for this adiabatic gate. However, they can be accounted for by solving the small set of density matrix equations that do *not* include the effect from axial recoil.

V. RESULTS

In this section, we present the results of calculations that test the accuracy of the approximations discussed above and in the Appendix and explore the behavior of the decoherence as a function of atomic parameters. We compare the approximations to the results from solving the full density matrix equations which automatically include all of the effects from photon absorption and reemission including changes in vibrational level, Doppler shifts, spatial changes, and momentum changes. Parameters will be chosen to correspond to transitions in Cs. All calculations in this section will use $M = 132.91$ atomic mass units. The excitation to the Rydberg state occurs from counter-propagating lasers of wavelength 459 and 1038 nm which gives an effective wavelength, $\lambda_{\rm eff} \simeq 822.9$ nm, for the photon kick, $K = 2\pi/\lambda_{\rm eff}$. For the effects from focusing, we will use a waist ($1/e^2$ intensity radius) of $w_0 = 2$ μm for each beam. This leads to Rayleigh ranges of 27.4 and 12.1 μm and an effective waist $w_0 = \sqrt{2}$ μm and effective Rayleigh range of 11.1 μm in Eq. (30).

We will use two example Rydberg states in the calculation, 66S and 106S. The lifetime of these states, 130 and 366 μs, respectively, include stimulated absorption and emission due to blackbody radiation [42,43].

A. π-2π-π C_Z gate

The first tests will involve parameters for the π-2π-π gate of Ref. [11]. To model the pulses, we use

$$\Omega_1(t) = \Omega_{1,\max}\left(e^{-(t+\tau_1/2)^6/\delta t_1^6} + e^{-(t-\tau_1/2)^6/\delta t_1^6}\right), \tag{39}$$

$$\Omega_2(t) = \Omega_{2,\max} e^{-t^6/\delta t_2^6}, \tag{40}$$

where the $\Omega_{j,\max}$ give the appropriate π pulses for atom 1 and 2π pulse for atom 2, $\tau_1 = 1.0044$ μs is the time between pulses for atom 1, $\delta t_1 = 0.14$ μs is the duration of each of the atom 1 pulses, and $\delta t_2 = 0.22$ μs is the duration of the atom 2

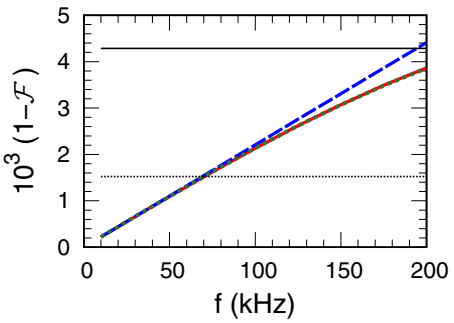

FIG. 3. The infidelity, $1-\mathcal{F}$ in Eq. (27), due to axial momentum kick for the atom in the ground state of a harmonic trap as a function of the trap frequency f, using $T=0$ and not including radiative decay of the Rydberg state. The trap potential is on for the full sequence, Eq. (39), for the parameters in the text. This calculation assumes the trapping potential is magic so that the potential is the same for all internal states. The solid red line is the full density matrix calculation, the long dashed blue line is from the approximation, Eq. (D5), and the green dotted line is the approximation that includes the trapping potential, Eq. (E4). The full density matrix calculation and Eq. (E4) are indistinguishable. The horizontal solid black line (66S) and dotted black line (106S) are the contribution to infidelity due to the finite lifetime (130 and 366 μs respectively) of these Rydberg states.

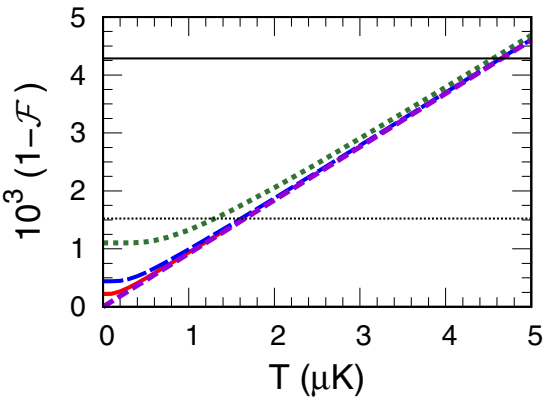

FIG. 4. The infidelity, $1-\mathcal{F}$, due to axial momentum kicks for the π-2π-π gate with the atom in a thermal distribution of a harmonic trap as a function of the temperature, T. The calculation does not include radiative decay of the Rydberg state. The different plots are for different trap frequencies: 10 (red solid), 20 (blue dashed), and 50 kHz (green dotted). The purple short dashed line is the high temperature approximation, Eq. (43), with the second term in the square brackets dropped. The approximation, Eqs. (41) and (D11), are indistinguishable from the full calculation on this scale. The horizontal lines are the same as Fig. 3.

pulse. Because of the order of magnitude difference between τ_1 and $\tau_2=\delta t_2/2$, the Bell state infidelity is $1-\mathcal{F}\simeq\varepsilon^{(1)}/2$.

Figure 3 shows the infidelity, $1-\mathcal{F}$ in Eq. (27), for these parameters as a function of the trapping frequency when the atoms start in the motional ground state. For this case, we assume a scenario where the trapping potential is magic so that the potential is the same for all states. The finite lifetime of the Rydberg state is *not included* in this calculation, but the horizontal lines show the contribution to the infidelity due to the Rydberg finite lifetime for 66S (solid) and 106S (dotted) states. The solid red line is from numerically solving the density matrix calculation; the approximation, Eq. (E4), that includes the trapping potential is the green dotted line that overlays the exact result. This shows that the small width of the individual π pulses has a negligible contribution to $\varepsilon^{(1)}$. The blue dashed line is the exact result when the trapping potential is turned off during the calculation, Eq. (D5). Because this calculation has $\sim$1 μs between π pulses, it is not surprising that Eq. (D5) becomes noticeably different from calculations with the trap on when $f\sim 100$ kHz. For these calculations, convergence to better than 0.01% was achieved using a maximum vibrational quantum number of 10.

It is, perhaps, a surprise that there is more, not less, decoherence as the trapping frequency increases. Intuition suggests that higher frequencies lead to less effects from atom recoil due to the larger energy spacing. However, because the durations are short, the size of the energy spacings are not relevant. The main effect is from the spatial size of the initial state and how far the atom moves during the sequence of laser pulses. The spatially smaller states at higher frequency have less overlap with the unkicked states. At the higher frequencies, the infidelity due to the axial photon kick can be larger than that from radiative losses even when the atom is in the motional ground state.

For the laser parameters of the previous paragraph, we now compare the approximation, Eq. (D11), to the full calculation with the trapping potential for a thermal distribution. Results from calculations with three different trap frequencies are shown in Fig. 4. These calculations include the trapping potential during the laser manipulations. The results from the approximation, Eq. (D11), are indistinguishable from the full solution on the scale shown indicating the trapping potential has little effect for these cases. As in Fig. 3, the horizontal lines are the infidelity due to finite Rydberg lifetime of the 66S (solid) and 106S (dotted) states. The fidelity is $\mathcal{F}>0.995$ for the temperatures plotted. The best value for the 50 kHz trapping potential is $\mathcal{F}\simeq 0.999$. The maximum number of vibrational states was used for the 20 kHz calculation at 5 μK because the 10 kHz calculation was only performed to 1.5 μK; the maximum number of vibrational states for this case was $\sim$100.

Figure 4 shows that the decoherence increases linearly with the temperature once k_BT is larger than $\sim\hbar\omega_\parallel$. Also, the decoherence is nearly independent of the frequency of the trapping potential when this condition is satisfied because the smallest relevant length scale is the thermal de Broglie wavelength. Since the approximation, Eq. (D11), is accurate, we can use it to derive an expression for the decoherence when $\varepsilon^{(1)}$ is small:

$$\varepsilon^{(1)}\simeq\frac{K^2\tau_1^2k_BT_{\rm eff}}{2M}=\frac{K^2\tau^2\hbar\omega_\parallel}{4M}\coth\left(\frac{\hbar\omega_\parallel}{2k_BT}\right),\tag{41}$$

where $\coth(x)=(e^x+e^{-x})/(e^x-e^{-x})$. The limits are

$$\varepsilon^{(1)}\to\frac{K^2\tau_1^2\hbar\omega_\parallel}{4M}[1+2e^{-\hbar\omega_\parallel/k_BT}]\quad\text{for } k_BT\ll\hbar\omega_\parallel\tag{42}$$

$$\to\frac{K^2\tau_1^2k_BT}{2M}\left[1+\frac{1}{12}\left(\frac{\hbar\omega_\parallel}{k_BT}\right)^2\right]\quad\text{for } k_BT\gg\hbar\omega_\parallel,\tag{43}$$

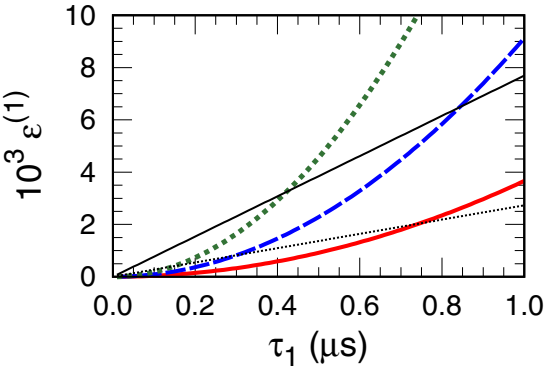

FIG. 5. The projection error, $\varepsilon^{(1)}$, due to axial momentum kick for atoms in a thermal distribution of a harmonic trap as a function of the time between π pulses. All calculations are for a trap frequency of 10 kHz using Eq. (41). The different plots are for different atom temperatures: 2 (red solid), 5 (blue dashed), and 10 μK (green dotted). The solid (66S) and the dotted (106S) black lines are $\Gamma\tau_1$.

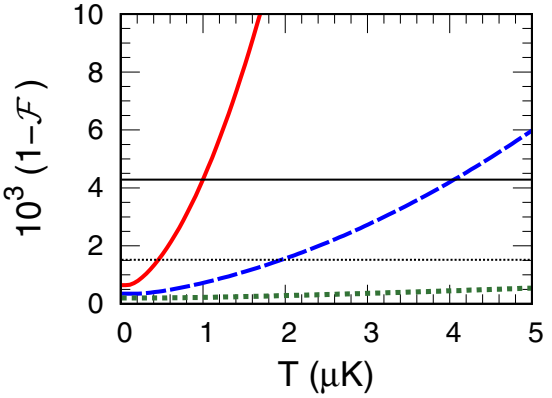

FIG. 6. The infidelity, $1-\mathcal{F}$, due to laser focus, Eq. (30), for the π-2π-π gate with the atom in a thermal distribution of a harmonic trap as a function of the temperature T. The calculation does not include radiative decay of the Rydberg state. The different plots are for different transverse trap frequencies: 10 (red solid), 20 (blue dashed), and 50 kHz (green dotted). This calculation does not include the axial decoherence since it is much smaller than that for the transverse degrees of freedom. The horizontal lines are the same as Fig. 3. A transverse misalignment of $y_0 = 100$ nm is assumed.

which shows the linear dependence on the temperature when the atoms are hot compared to the quantum energies. It also shows that the decoherence does not depend on the trap frequency at high temperatures. Another point of comparison is to remember that the average number of vibrational quanta is $\langle n\rangle = 1/\{\exp[\hbar\omega_\parallel/(k_BT)]-1\}$. When $k_BT = \hbar\omega_\parallel$, the average vibrational quanta is $\langle n\rangle \simeq 0.58$ and the fractional error in the high temperature form of the decoherence is 8%. When $k_BT = 2\hbar\omega_\parallel$ then $\langle n\rangle \simeq 1.54$ and the fractional error is 2%. This illustrates how quickly the trap frequency becomes irrelevant to the decoherence.

As a physical example, we consider the case from Ref. [13] where Sr is excited from the $^3P_0$ metastable state to $^3S_1$ Rydberg states using a single 317 nm photon. The time scale for a 2π pulse was of order 100 ns. Using their estimated temperature of $2.5/\sqrt{10}$ μK $= 0.8$ μK gives $\varepsilon^{(1)} \simeq 1.5\times10^{-4}$. However, if the gate is composed of more than one pulse, the duration can be longer. The decoherence increases to $\varepsilon^{(1)} \simeq 1.3\times10^{-3}$ if $\tau_1 = 300$ ns.

The scale of the projection error can be compared to the decoherence from decay of the Rydberg state. Figure 5 shows the $\varepsilon^{(1)}$ for calculations in a 10 kHz trap for three different temperatures (2, 5, and 10 μK) as a function of the time, τ_1, between the π pulses. Comparing this time scale and trap frequency to that in Fig. 3, whether the trap is on or off during these operations has no visual effect on the results. This emphasizes that the infidelity from Rydberg state decay scales linearly with τ_1 while that from recoil is proportional to the square of the time. For short times between pulses, the main error will be due to the decay of the Rydberg state. For pulses with $\tau_1 \sim 1$ μs, the atoms need to be cold for the projection error to be smaller than the decay probability.

The infidelity due to laser focusing, Eq. (30), does not depend on the duration of the gate as long as the duration is much less than the trap period. The results with the trap on were visually indistinguishable from those with the trap off for Figs. 6 and 7. This infidelity has the strongest dependence on the effective temperature of the mechanisms examined in this paper. Figure 6 shows the infidelity, Eq. (30), for 3 different transverse trap frequencies: 10 (solid red), 20 (blue dashed), and 50 kHz (green dotted). For this calculation and that of Fig. 7, we assumed the terms with x_R are less than 10% of the transverse decoherence and have been dropped. The effective waist is $\sqrt{2}$ μm and there is assumed misalignment of $y_0 =$ 100 nm. This figure illustrates how sensitive the infidelity is to the transverse trap frequency: at high temperature, the infidelity is proportional to $1/f_\perp^4$. This figure also shows how high temperature exacts a high penalty because the infidelity scales like T^2 in this limit.

Figure 7 shows how the axial displacement, y_0, can quickly degrade the fidelity of the π-2π-π gate. This graph uses

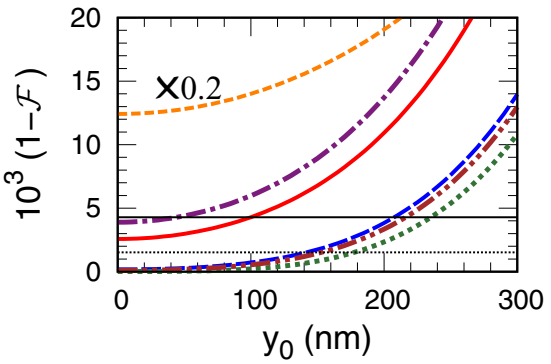

FIG. 7. The infidelity, $1-\mathcal{F}$, due to laser focus, Eq. (30), for the π-2π-π gate with the atom in a thermal distribution of a harmonic trap as a function of the displacement, Y_0. The calculation does not include radiative decay of the Rydberg state. The different plots are for different transverse trap frequencies and temperatures: 10 kHz, 1 μK (red solid), 20 kHz, 1 μK (blue dashed), and 50 kHz, 1 μK (green dotted), 10 kHz, 5 μK (orange short dash), 20 kHz, 5 μK (purple dash-dot), and 50 kHz, 5 μK (brown dash-dot-dot). The 10 kHz, 5 μK infidelity is divided by 5 to fit on the same graph. This calculation does not include the axial decoherence since it is much smaller than that for the transverse degrees of freedom. The horizontal lines are the same as Fig. 3.

the same parameters as Fig. 6 except the temperatures and frequencies are fixed: the curves use 10, 20, or 50 kHz and 1 or 5 μK. As with Fig. 6, it is clear that larger temperatures dramatically degrade the fidelity as do lower trap frequencies. Figure 7 demonstrates the importance of alignment for the gate fidelity since the infidelity, Eq. (30), has a quartic dependence on y_0. It is interesting that the infidelity from displacement of the focused beam is greater than that due to finite Rydberg lifetime for displacements larger than ~200 nm even for the 66S state; this value is ~1/10 the waist of the individual beams.

Because the infidelity is proportional to the atom temperature for $k_BT > \hbar\omega$, the change in vibrational character due to gate pulses should be examined. This effect can be estimated using the heating of the atom's center of mass motion due to the time delay between the pulses. The kick shifts the position which leads to heating. For reasonable gate parameters, this effect will be negligible except for high frequency traps at the lowest temperatures. The center of mass energy will change by the amount

$$\Delta E = \frac{1}{2}M\omega^2\delta x^2 = \frac{\hbar^2K^2}{2M}(\omega\tau_1)^2, \tag{44}$$

which is the recoil energy times $(\omega\tau_1)^2$. Since $\omega\tau_1$ will be much less than one, this shows the energy will increase by a small fraction of the recoil energy per gate. To give an idea of the size of the two effects, for $\tau_1 = 1.00$ μs and $\lambda_{\rm eff} =$ 822.9 nm, the change in energy from Eq. (44) is 0.42 nK per kick for a 10 kHz trap, 1.7 nK per kick for 20 kHz, and 11 nK per kick for 50 kHz.

As a comparison, the change in energy that occurs when the trap is turned off for a time $\tau \simeq \tau_1 + 4\delta t_1 \simeq 1.56$ μs and then turned back on is $\Delta E = (k_BT_{\rm eff}/2)(\omega\tau)^2$. For this effect, the size of the energy change increases with each time the trap is turned off and back on. Taking $< E >= k_BT_{\rm eff}$, The temperature after N gates is $T_N = T_{\rm eff}\exp[N(\omega\tau_1)^2/2]$. For 100 gates, $T = T_{\rm eff}e^{0.48} = 1.62T_{\rm eff}$ for a 10 kHz trap, $e^{1.92}T_{\rm eff} = 6.83T_{\rm eff}$ for a 20 kHz trap, and $e^{12}T_{\rm eff} = 1.6\times10^5T_{\rm eff}$ for a 50 kHz trap. Clearly, several approximations break down for the 50 kHz trap before this limit is reached. Nevertheless this result indicates that turning on and off a 50 kHz trap is not a good idea. Fortunately it is possible to design traps that present the same trapping potential for ground and Rydberg atoms so it is feasible to leave the trap potential on continuously [44].

B. Adiabatic C_Z gate

This section contains results for the adiabatic gate discussed in Sec. IV D. Examples of parameters that lead to an effective C_Z gate are in Table I. The values for τ_1, Eq. (D16), result from one atom calculations and τ_R, Eq. (34), result from two atom calculations that do not include atomic recoil. The values for $1-\mathcal{F}$ in this table result from calculations that do not include the atomic recoil but do include the radiative loss from the Rydberg state. In Table I, the infidelity is almost completely due to the radiative loss; the number of photons absorbed or emitted is equal to the infidelity to the digits given. If the radiative loss is *not* included, the infidelity solely arises from nonadiabaticity and from nonideal choice of gate parameters to generate a C_Z gate; ignoring radiative loss, the infidelity would be 1.8×10^{-5}, 9.9×10^{-8}, and 1.3×10^{-5} for the three cases shown.

TABLE I. Parameters for the adiabatic gate. All have $\Omega_0 = 2\pi\times17$ MHz. Parameters τ_1, τ_R are defined in Eqs. (D16) and (34). The infidelity $1-\mathcal{F}$ is that due to the pulse shapes, finite blockade, and includes finite Rydberg lifetime, but does *not* include momentum kicks, i.e. the atoms are fixed in space for the determination of the gate parameters. The left infidelity is for 66S and the right is for 106S. See Fig. 8 for an example that includes momentum kicks.

Gate	Δ/Ω_0	δt (μs)	B (10^6s^{-1})	τ_1, τ_r (ns)	$1-\mathcal{F}$ (10^{-4})
1	−0.5000	0.2	2π 600	90, 63	6.3, 2.4
2	−0.8635	0.2165	2π 60	56, 42	3.8, 1.3
3	−0.3000	0.5	2π 4	357, 416	30, 11

Compared to the gate in the previous section, the resulting duration in the Rydberg state, $\tau_{1,R}$, is over an order of magnitude shorter for gates 1 and 2 and a factor of ~3 smaller for gate 3. This should translate to a factor of ~100 (gates 1 and 2) or ~10 (gate 3) improvement in fidelity due to momentum kicks with a factor of ~10 and ~3 improvement of radiative decay of the Rydberg state.

Figure 8 shows the infidelity including the effect from momentum kicks, $1-\mathcal{F}$, versus the atom temperature for gate 3 which is the worst gate in the table because it assumes the weakest Rydberg interaction and therefore requires a relatively long interaction time leading to more spontaneous emission. The calculation is performed for a trapping frequency of 50 kHz to reduce the size of the density matrix calculation. Higher temperature or lower frequency requires more states for convergence. The trap is on for the duration of the gate but there is no visual difference if the trap is off due to the short duration of the gate compared to the trap period. The two atom kick calculations have up to 40 vibrational states for each atom for the 5 μK calculation and goes to tenth order in the expansion of the exponential e^{iKx}.

As expected, the infidelity is a factor of ~10 smaller than the gates of the previous section. The full results were compared to the simple expression Eq. (38), with the intrinsic

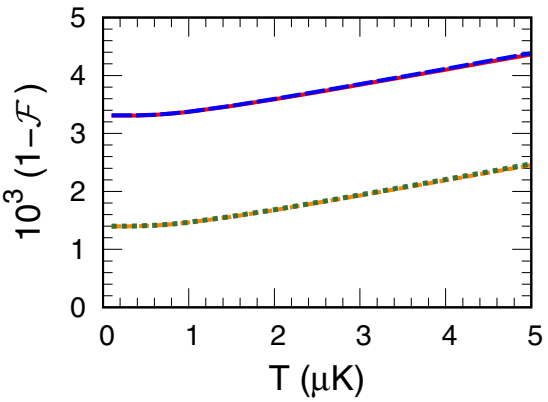

FIG. 8. The Bell state infidelity for gate 3, see Table I, as a function of atom temperature. The trap has a frequency of 50 kHz. The solid red line is from the full density matrix calculation and the dashed blue line is from Eq. (38) added to the intrinsic $1-\mathcal{F}$ from Table I for 66S. The orange short dash and green dotted are the same for 106S.

gate error of Table I added to it. As seen in the figure, there is good agreement between the full calculation and the simple analytic results. In this temperature range, the main infidelity for this gate is due to radiative losses in the Rydberg state. The infidelity from the momentum kicks becomes larger than that from radiative losses at temperatures a bit above 10 μK.

In this gate, population does transiently occupy the double Rydberg state which means there can be additional entanglement between the internal states and the motional character due to Rydberg - Rydberg forces as discussed in Sec. II B. Examining the projections in Eq. (23), the definition of Bell state fidelity in Eq. (19), and the overlap factor in Eq. (7), a van der Waals interaction contributes a decrease to the fidelity of

$$1-\mathcal{F}=\frac{3}{8}[1-\langle\psi_{f,00}|\psi_{f,11}\rangle]=\frac{27\mathsf{B}^2k_BT_{\rm eff}\tau_{RR}^2}{2M\omega_\perp^2 r_{12}^2}, \qquad (45)$$

where the parameters are defined below Eq. (7) and the thermal average was taken in the expectation value of Eq. (7). For $1/r_{12}^3$ interactions, this expression should be divided by 4. Unlike the momentum kick from the photon, the trap frequency explicitly appears in the infidelity. As the trap frequency increases, the infidelity decreases as expected.

This expression was checked by solving the full density matrix equations for gates 2 and 3 for several temperatures and found to be accurate at the couple percent level. Calculations gave τ_{RR} of 31.6 ps, 8.60 ns, and 157 ns for gates 1, 2, and 3. For gate 1, the separations r_{12} are 2.6 and 5.3 μm for the 66S and 106S states, respectively, while for gate 2 the separations are 4.2 and 10.5 μm and for gate 3 are 8.0 and 20.0 μm. The crossover distance [45] between a resonant dipole-dipole interaction scaling as $1/r_{12}^3$ and a van der Waals interaction scaling as $1/r_{12}^6$ increases with the principal quantum number and we find it to be approximately 2 μm for the 66S state and 8 μm for the 106S state. Therefore gate 1 has $1/r_{12}^3$ interaction strength while gates 2 and 3 have $1/r_{12}^6$. For $T_{\rm eff}=5$ μK and 50 kHz trap frequency, the infidelities are (gate 1: 2.2×10^{-5}, 5.4×10^{-6}), (gate 2: 2.5×10^{-2}, 4.1×10^{-3}), and (gate 3: 1.0×10^{-2}, 1.7×10^{-3}).

VI. CONCLUSIONS

We have derived the equations needed to analyze the decoherence that arises from the entanglement of internal states of neutral atoms with the motional degrees of freedom. The entanglement occurs when the internal states of the atom are manipulated by laser pulses. Although entangled atomic states can be prepared using collisional interactions without resorting to laser excitation, Rydberg gates have the advantage that they are fast, operate at long range, and can reach high fidelity without preparation of atoms in the motional ground state.

Different levels of approximation were considered above and it was shown that a sudden approximation well describes the decoherence in this system. This approximation gives a simple formula for the decoherence, Eq. (D4), in terms of the shift in position due to the photon absorption and re-emission, δx, and an initial state length scale Δx. We also derived the infidelity that occurs when the lasers that excite the atom are focused.

The trends in the decoherence are important for future experiments, especially in the limit of small decoherence $\varepsilon \ll 1$. The decoherence is quadratic in the shift in position due to the absorption and re-emission of the photons which means the decoherence is quadratic in the separation of laser pulses, τ, and in the momentum kick from the photon, $\hbar K$. It is also inversely quadratic in the initial state length scale Δx; larger Δx leads to less decoherence and vice versa. For cold atoms, the initial state length scale is that for a harmonic oscillator which is inversely proportional to the trap frequency. This leads to the decoherence being proportional to the trap frequency at low temperatures. At high temperatures, this length scale is the thermal de Broglie wave length which is inversely proportional to the temperature. This leads to the decoherence being proportional to the temperature at high temperatures. Finally the combination that δx is inversely proportional to the mass and Δx is inversely proportional to the square root of the mass leads to the decoherence being inversely proportional to the mass.

The direction of the trends are as might be expected with the possible exception that the decoherence is less for small trap frequencies (i.e., it is not necessary to get into the motional ground state, but it is necessary to be cold). The particular power law of the dependence might not be expected and shows where it is important to do better. For example, if the momentum kick is decreased by a factor of 2 by using a pair of counter-propagating photons, the decoherence will decrease by a factor of 4. The trends discussed above and the simple expression for the decoherence will be a useful guide for quantum computation applications.

For focused lasers the π-2π-π gate infidelity increases with the deviation of the atomic position from the focal position of the excitation beam. Inspection of Eq. (F5) shows that there is a temperature independent error associated with misalignment of the trapping potential and the excitation laser, followed by contributions that scale as temperature and temperature squared. The temperature dependent errors are inversely proportional to the trap frequency to the second and fourth powers. We have not analyzed the focusing error for the adiabatic gate, but anticipate that it will be significantly smaller due to the insensitivity of the adiabatic pulse area to the laser amplitude [26].

The trend for the focusing error is that it is less for larger transverse trap frequencies. This is opposite to the motional infidelity which favors lower axial trap frequencies. This the case for the π-2π-π gate and the adiabatic gate analyzed here. Similar trends are expected for other gate protocols. The expressions derived for the dependence of gate infidelity on trap parameters, atomic temperature, and pulse parameters will be useful for reaching high fidelity regimes needed for quantum information applications.

ACKNOWLEDGMENTS

F.R. was supported by the National Science Foundation under Grant No. 1804026-PHY. The work at UWM was supported by NSF PHY-1720220, NSF Award 2016136, ARL-CDQI Cooperative Agreement No. W911NF-15-2-0061, DOE Award DE-SC0019465, and DARPA Contract No. HR001120C0068.

APPENDIX A: ANALYTIC RESULTS FOR 1 ATOM

Basic equations

The derivation in this section will be based on the Schrödinger equation to simplify the interpretation. All of the calculated results, Sec. V, were found by numerically solving the full density matrix equation, Eq. (13), except for those presented in Figs. 6 and 7.

To solve for the decoherence measured by χ, Eq. (5), the full Schrödinger equation needs to be tracked through the different excitation and de-excitation steps. By solving the full Schrödinger equation, we automatically include all of the effects like changes in vibrational level, Doppler shifts, spatial changes, and momentum changes. For a three-state atom, the three state wave function will be written as

$$|\Psi(t)\rangle = \sum \psi_j(x,t)|j\rangle e^{-i\mathcal{E}_j t/\hbar}, \tag{A1}$$

where $\mathcal{E}_j$ is the energy of internal state $|j\rangle$ and we have incorporated the C_j's into the spatial function to make the notation simpler. The spatial functions are solutions of the equations

$$\begin{aligned} i\hbar\frac{\partial\psi_0}{\partial t} &= H_{C,0}\psi_0, \\ i\hbar\frac{\partial\psi_1}{\partial t} &= H_{C,1}\psi_1 + V_{1R}e^{-i\omega_{R1}t}\psi_R, \\ i\hbar\frac{\partial\psi_R}{\partial t} &= H_{C,R}\psi_R + V_{1R}e^{i\omega_{R1}t}\psi_1, \end{aligned} \tag{A2}$$

where the $H_{C,j}$ is the kinetic energy operator plus the trapping potential for state $|j\rangle$, $V_{1R}(x,t) = \hbar\Omega(t)\cos(\bar{\omega}t - Kx)$ is the coupling between internal states $|1\rangle$ and $|R\rangle$ due to the laser, K is the wave number of the photon, and $\omega_{R1} = (\mathcal{E}_R - \mathcal{E}_1)/\hbar$. The $\Omega(t)$ is the Rabi frequency for the 1-R transition. The frequency of the laser, $\bar{\omega}$, might also have time dependence if the laser is chirped.

The rotating wave approximation should work very well for this system since the transition frequency is large and the laser is weak. This leads to the approximation

$$\begin{aligned} i\hbar\frac{\partial\psi_1(x,t)}{\partial t} &= H_1\psi_1(x,t) + \frac{\hbar\Omega(t)}{2}e^{-iKX}\psi_R(x,t), \\ i\hbar\frac{\partial\psi_R(x,t)}{\partial t} &= H_r\psi_R(x,t) + \frac{\hbar\Omega(t)}{2}e^{iKX}\psi_1(x,t), \end{aligned} \tag{A3}$$

where the $e^{\pm iKx}$ leads to the momentum kicks during the absorption and stimulated emission steps. These equations can be solved numerically using many different techniques, leap-frog, Crank-Nicolson, etc. In cases where we numerically solved the Schrödinger equation, we used the leapfrog algorithm for the time propagation.

The situation described above has the *initial* $\psi_1(x,t) = C_1\psi_{\text{in}}(x)$ and $\psi_R(x,t) = 0$. After the pair of laser pulses, the $\psi_R(x,t) \simeq 0$. There is some population left in state $|R\rangle$ due to Doppler shifts of the wave function but the population is small for the cases discussed in this manuscript. The full calculations automatically includes the population left in the Rydberg state as well as the phase changes due to atomic motion. The approximations described below ignore the population left in the Rydberg state but give analytic expressions for the phase changes correct to lowest nonzero order in v/c within the limits given for each approximation.

The amplitude $\Omega(t)$ is chosen to give approximately 100% transition from 1-to-R and from R-to-1. This condition can be accomplished in a variety of ways: a single 2π pulse, two π pulses, etc. For example, a simple form that satisfies these requirements and models excitation to the Rydberg state with a time delay τ before de-excitation is

$$\Omega(t) = \frac{\sqrt{\pi}}{\delta t}\left(e^{-t^2/\delta t^2} + e^{-(t-\tau)^2/\delta t^2}\right). \tag{A4}$$

APPENDIX B: NO TRAPPING POTENTIAL, $V_{\text{tr}} = 0$

In many experiments, the trapping potential for the atom will be dropped during the laser excitation and de-excitation steps. In this situation, the $H_{C,0} = H_{C,1} = H_{C,R} = P^2/(2M)$. This may seem a special case, but in most experiments it is expected that the total duration of all laser pulses will be much shorter than the oscillation period of the trapping potential. We found that using the approximation $V_{\text{tr}} = 0$ in this case also led to accurate results for the momentum kicks.

Equations (A3) can be recast using the Fourier transform

$$\phi_j(k,t) = \frac{1}{\sqrt{2\pi}}\int_{-\infty}^{\infty} e^{-ikx}\psi_j(x,t)dx \tag{B1}$$

by multiplying from the left by $\exp(-ikx)/\sqrt{2\pi}$ and integrating over x. This gives the Schrödinger equation for the Fourier transforms

$$\begin{aligned} i\hbar\frac{\partial\phi_1(k,t)}{\partial t} &= E(k)\phi_1(k,t) + \frac{\hbar\Omega(t)}{2}\phi_R(k+K,t), \\ i\hbar\frac{\partial\phi_R(k,t)}{\partial t} &= E(k)\phi_R(k,t) + \frac{\hbar\Omega(t)}{2}\phi_1(k-K,t), \end{aligned} \tag{B2}$$

where $E(k) = \hbar^2k^2/(2M)$ is the kinetic energy. This may appear to be just as complicated to solve as the Schrödinger equation in x, Eqs. (A3), but it is actually much simpler. By writing the second equation at $k+K$, every k corresponds to a simple two-state system. The k-space equations, Eq. (B2), reduce to $\mathcal{N}_k$ pairs of equations where $\mathcal{N}_k$ are the number of k points in $\phi_j(k,t)$. We label the functions on a grid in k using equally spaced points $k_i = k_0 + i\cdot\delta k$ where $i = 0, 1, \ldots, \mathcal{N}_k - 1$ as $\phi_{1,i}(t) = \phi_1(k_i,t)$ and $\phi_{R,i}(t) = \phi_R(k_i + K,t)$. Note the $\phi_{R,i}$ are at shifted momenta compared to the $\phi_{1,i}$ This results in the set of equations

$$\begin{aligned} i\hbar\frac{\partial\phi_{1,i}(t)}{\partial t} &= E(k_i)\phi_{1,i}(t) + \frac{\hbar\Omega(t)}{2}\phi_{R,i}(t), \\ i\hbar\frac{\partial\phi_{R,i}(t)}{\partial t} &= E(k_i+K)\phi_{R,i}(t) + \frac{\hbar\Omega(t)}{2}\phi_{1,i}(t), \end{aligned} \tag{B3}$$

where the energy is shifted in the second equation to account for the shift in the $\phi_{R,i}$ [19].

Because these equations do not couple the ϕ at different i, a massive simplification in the calculation of the decoherence occurs. The final ϕ can be written in terms of the initial ϕ and a unitary rotation that depends on, i:

$$\phi_{j,i}(t_f) = \sum_{j'} U_{jj'}(i;t_f,t_0)\phi_{j',i}(t_0), \tag{B4}$$

where t_0 is the initial time and t_f is the final time The simplification arises because the decoherence projection χ only

depends on the $U_{11}(i;t_f,t_0)$ projected on the initial state. Since the overlaps do not depend on the representation

$$\chi = \int_{-\infty}^{\infty} \phi_{f,0}^*(k)\phi_{f,1}(k)dk \simeq \delta k \sum_i |\phi_{\text{in},i}|^2 e^{iE(k_i)(t_f-t_0)/\hbar} U_{11}(i;t_f,t_0), \quad \text{(B5)}$$

where the initial function is $\phi_{\text{in},i} = \phi_{\text{in}}(k_i)$ and we used the fact that the $\phi_{0,i}(t) = \exp(-iE(k_i)t/\hbar)\phi_{\text{in},i}(0)$. Thus, within the rotating wave approximation and the discretization of the k-space wave functions, the decoherence overlap is given by

$$\chi = \sum_i \delta k |\phi_{\text{in},i}|^2 \mathcal{K}_{11}(i), \quad \text{(B6)}$$

where $\mathcal{K}_{11}(i) = \exp(iE(k_i)(t_f-t_0)/\hbar)U_{11}(i;t_f,t_0)$ is the kernel for the momentum k_i to start in state $|1\rangle$ at time t_0, propagate forward in time to t_f with the laser pulses, and then propagate backward in time to t_0 with no laser pulses.

APPENDIX C: THERMAL DISTRIBUTION: $V_{\text{tr}} = 0$

Using the theoretical development of the previous section, the decoherence overlap for a thermal distribution is derived in this section. The initial system is an incoherent sum over eigenstates, $\phi_\alpha(k)$, with the probability of each state being $P_\alpha = \exp(-E_\alpha/[k_BT])/Z$ with $Z = \sum_\alpha \exp(-E_\alpha/[k_BT])$. One way to treat this is to say that the initial state is

$$\phi_{\text{in},i} = \sum_\alpha \sqrt{P_\alpha} e^{i\theta_\alpha} \phi_\alpha(k_i), \quad \text{(C1)}$$

where the phases θ_α are random. This leads to the decoherence overlap being

$$\chi = \sum_i \delta k \mathcal{K}_{11}(i) \sum_{\alpha\alpha'} \sqrt{P_\alpha P_{\alpha'}} \phi_\alpha(k_i)\phi_{\alpha'}(k_i) e^{i(\theta_\alpha-\theta_{\alpha'})} = \sum_i \delta k \mathcal{K}_{11}(i)\rho(k_i,k_i), \quad \text{(C2)}$$

where the k-space density matrix is

$$\rho(k_i,k_i) = \sum_\alpha P_\alpha \phi_\alpha^2(k_i) \quad \text{(C3)}$$

arises because all of the cross terms in α,α' average to 0. Thus, for the cases where the trapping potential can be neglected during the laser manipulations, the decoherence for a thermal distribution is just as easy to obtain as for a particular state.

The density matrix in Eq. (C2) depends on the temperature and the potential the atoms were trapped in just before the laser manipulations occur. Typically, this is a nearly harmonic potential.

The density matrix for a thermal distribution in a harmonic oscillator can be exactly obtained for any temperature. The Wigner function for a thermal distribution is

$$W(x,k) = C\exp(-[\Delta k x]^2 - [\Delta x k]^2), \quad \text{(C4)}$$

where $\Delta k^2 = M\omega^2/(2k_BT_{\text{eff}})$, $\Delta x^2 = \hbar^2/(2Mk_BT_{\text{eff}})$, and the T_{eff} is defined in Eq. (C7). The M is the atomic mass, k_B is Boltzmann's constant, and T_{eff} is an effective temperature given below. The density matrix can be obtained by Fourier transform

$$\rho\left(k+\frac{\bar{k}}{2}, k-\frac{\bar{k}}{2}\right) = \int e^{-i\bar{k}x} W(x,k)dx = \frac{\Delta x}{\sqrt{\pi}} \exp\left(-[\Delta x k]^2 - \frac{\bar{k}^2}{4\Delta k^2}\right) \quad \text{(C5)}$$

and a similar expression can be obtained for the spatial density matrix by Fourier transforming on k. Although tedious, one can show that this is the exact density matrix by using $\rho_T = C\rho_{2T}\rho_{2T}$.

The diagonal density matrix is obtained by setting $\bar{k} = 0$:

$$\rho(k,k) = \frac{\hbar}{\sqrt{2\pi M k_B T_{\text{eff}}}} \exp(-\hbar^2k^2/[2Mk_BT_{\text{eff}}]), \quad \text{(C6)}$$

where we have substituted for Δx. The T_{eff} can be fixed by forcing the average energy from the classical form, $\bar{E} = k_BT_{\text{eff}}$, to equal the average energy from the quantum thermal distribution,

$$k_BT_{\text{eff}} = \hbar\omega\left(\frac{1}{2} + \frac{1}{e^{\hbar\omega/(k_BT)}-1}\right). \quad \text{(C7)}$$

which gives the limit $k_BT_{\text{eff}} \to \hbar\omega/2$ at low temperatures and $k_BT_{\text{eff}} \to k_BT$ at high temperatures.

Thus, the decoherence overlap for a thermal distribution is obtained by using the result of Eqs. (C6) and (C7) in Eq. (C2).

APPENDIX D: OVERLAPS FOR $V_{\text{tr}} = 0$

This section derives approximate expressions for the decoherence overlap for different excitation/de-excitation procedures. All cases assume the center of mass coordinate is in a thermal distribution and that the trapping potential is off during the gate. The latter condition is a good approximation if the gate duration is short compared to the trapping period. We note that having the atom in the motional ground state is a thermal distribution with $T \to 0$ which gives $k_BT_{\text{eff}} \to \hbar\omega/2$. We account for the atom recoil during the stimulated absorption and emission process in all of the cases.

1. Short, 2π pulse, on resonance

This section derives the χ when there is a single, short pulse that takes 100% of the atom population from state $|1\rangle$ to the Rydberg state and back to state $|1\rangle$. If the atom is treated as stationary, this leads to a π phase shift for state $|1\rangle$. We assume that the duration of the laser pulse is short enough that the band width of the laser is much larger than the Doppler width and the spacing of the energy levels. In this limit, the shape of the pulse is not important and we choose for it to be a flat top function:

$$\Omega(t) = \frac{2\pi}{\delta t} \quad 0 \leqslant t \leqslant \delta t \quad \Omega(t) = 0 \text{ otherwise.} \quad \text{(D1)}$$

For this $\Omega(t)$, Eqs. (B3) can be solved exactly. Defining the parameters

$$\delta E_i = E(k_i+K) - E(k_i), \quad \bar{E}_i = \frac{E(k_i+K)+E(k_i)}{2}, \quad \text{(D2)}$$

the final population in the state $|1\rangle$ is 1 minus a term of order $(\delta E \delta t/\hbar)^4$ so it is only the phase dependence that contributes to χ. We find

$$\mathcal{K}_{11}^{(2)}(i) \simeq -e^{-i\delta E_i \tau_2/\hbar}, \tag{D3}$$

where we have defined $\tau_2 = \delta t/2$ is the time spent in the Rydberg state.

We can use this approximation with the thermal density matrix, Eq. (C6), to obtain an analytic expression for the decoherence overlap. The energy difference is $\delta E_i = E_{\rm rec} + \hbar^2 k_i K/M$ where $E_{\rm rec} = \hbar^2 K^2/(2M)$ is the recoil energy of the atom. Thus, the overlap is reduced to the Fourier transform of a Gaussian giving:

$$\chi^{(2)} = -e^{-iE_{\rm rec}\tau_2/\hbar} e^{-(\delta x/[2\Delta x])^2}, \tag{D4}$$

where $\delta x = \hbar K \tau_2/M$ is the distance an atom shifts due to the absorption and re-emission of photons separated in time by τ_2 and $\Delta x = \hbar/\sqrt{2k_B T_{\rm eff} M}$ is proportional to the de Broglie wave length at the effective temperature $T_{\rm eff}$ in Eq. (C7).

This form leads to a nice interpretation of the decoherence. The phase has a -1 from the pulse and has an accumulation that arises from the average change in kinetic energy of the atom due to the photon absorption, $E_{\rm rec}$, for photons separated by τ_2. The decrease in normalization arises because the atoms shift position due to their changed velocity over the duration τ_2. At low temperatures, the shift is compared to the spatial width of the ground state wave packet because $k_B T_{\rm eff} \simeq \hbar\omega/2$. At higher temperatures, the shift is compared to the coherence length of the atomic packet which is proportional to the thermal de Broglie wave length.

If the phase is corrected, this gives a value

$$\varepsilon^{(2)} \simeq \left(\frac{\delta x}{2\Delta x}\right)^2 = \frac{K^2 \tau_2^2 k_B T_{\rm eff}}{2M} \tag{D5}$$

where the Taylor series expansion of the Gaussian in Eq. (D4) was used because the duration is short. This result shows that ε for this case is proportional to: the square of the duration of the pulse, the effective temperature, $T_{\rm eff}$ in Eq. (C7), the square of the photon momentum, and the inverse of the atom mass. This suggests which parameters can be used to suppress decoherence due to momentum kick. For example, a one photon excitation with 319 nm photons is approximately 6.6 times worse than excitation with counter propagating 459 and 1038 nm photons.

2. Two short, π pulses, on resonance

This section derives the effect from a case like in Eq. (A4). We will assume τ is much less than the period of center of mass motion.

As a first approximation, we treat the case where the $\delta t \ll \tau_1$ which allows a very simplified derivation. In this case, we treat the excitation and de-excitation steps as being instantaneous and can be thought of as a sudden approximation. The final wave function is obtained from the concatenation of three steps. The first step is the excitation from state $|1\rangle$ to $|R\rangle$ with the momentum kick:

$$\phi_R(k+K) = -i\phi_{{\rm in},1}(k), \tag{D6}$$

where the $-i$ results from the π pulse. The second step is the free evolution of state $|R\rangle$ for a time τ_1:

$$\phi_R(k+K) = -i\phi_{{\rm in},1}(k) e^{-iE(k+K)\tau_1/\hbar}, \tag{D7}$$

where the phase accumulation is at the shifted momentum. The third step is the de-excitation giving:

$$\phi_{f,1}(k) = (-i)^2 \phi_{{\rm in},1}(k) e^{-iE(k+K)\tau_1/\hbar}, \tag{D8}$$

where the $-i$ again results from the π pulse. This gives the sudden approximation of the kernel:

$$\mathcal{K}_{11}^{(1)} = -e^{-i[E(k+K)-E(k)]\tau_1/\hbar}. \tag{D9}$$

This is the same form as Eq. (D3) which means the χ also has the same form:

$$\chi^{(1)} = -e^{-iE_{\rm rec}\tau_1/\hbar} e^{-(\delta x/[2\Delta x])^2} \tag{D10}$$

with the parameters as defined below Eq. (D4). The interpretation is the same as below Eq. (D4) and has the same type of scaling. As in the previous section, if the phase is corrected this gives a value

$$\varepsilon^{(1)} = \left(\frac{\delta x}{2\Delta x}\right)^2 = \frac{K^2 \tau_1^2 k_B T_{\rm eff}}{2M}, \tag{D11}$$

where τ_1 is the time between π pulses. This expression has the same form as in the previous section and, thus, has the same scaling. In most applications, the separation of the pulses is at least a few times longer than the duration of the pulses. Since the $\varepsilon^{(1)}$ is proportional to τ_1^2, this suggests that gates based on excitation followed by a delay and then de-excitation will have larger decoherence due to photon kick.

To extend the applicability to $\delta t < \tau$, the derivation from Sec. D 1 can be repeated but with two pulses with strength $\pi/\delta t$ centered at $t = 0$ and τ_1. Ignoring the terms of order $(\delta E \delta t/\hbar)^4$ as in the previous section, a full derivation gives exactly the same value as Eq. (D9). This can be seen because the two pulses give a phase accumulation of $-\delta E_i(2\delta t)/2$ and the time between the pulses gives a phase accumulation of $-\delta E_i(\tau_1 - \delta t)$. Thus, the result in Eq. (D11) does not depend on the sudden approximation and is more accurate than might be expected.

3. One adiabatic pulse

Instead of exciting the Rydberg state, some gates have a laser pulse that is detuned so that the population adiabatically evolves, ~100% of the population is in state $|1\rangle$ at the end of the pulse. This is apparently quite different from the previous two cases, because the admixture of Rydberg state can be small and "virtual" when the detuning is large. However, the derivation below shows that the same form for ε results.

For this case, there is a detuning, Δ of the laser from $\hbar\omega_{R1}$ so the Eq. (B3) is modified to

$$\begin{aligned} i\hbar\frac{\partial\phi_{1,i}(t)}{\partial t} &= \left(\bar{E}_i + \frac{\hbar\Delta - \delta E}{2}\right)\phi_{1,i}(t) + \frac{\hbar\Omega(t)}{2}\phi_{R,i}(t), \\ i\hbar\frac{\partial\phi_{R,i}(t)}{\partial t} &= \left(\bar{E}_i - \frac{\hbar\Delta - \delta E}{2}\right)\phi_{R,i}(t) + \frac{\hbar\Omega(t)}{2}\phi_{1,i}(t). \end{aligned} \tag{D12}$$

Because the gate is adiabatic, the final probability in $|1\rangle$ is $\simeq 1$ so only the difference in the phase accumulated in $\phi_{1,i}$ compared to $\phi_{0,i}$ is important. This will lead to

$$\mathcal{K}_{11} = \mathcal{K}_{11}(\delta E = 0)e^{-i\alpha}. \tag{D13}$$

If α can be written in the form $\alpha = \delta E \tau_a/\hbar$, then this example will have the same form and interpretation as the previous two sections. To calculate α, we integrate the time dependent difference between the adiabatic energy and that with $\delta E = 0$ and the phase accumulated in $\phi_{0,i}$:

$$\alpha = \frac{1}{\hbar}\int_{-\infty}^{\infty}\left[\frac{\mathrm{sgn}(\Delta)}{2}\sqrt{(\hbar\Delta - \delta E)^2 + \hbar^2\Omega^2} + \bar{E} - \frac{\hbar\,\mathrm{sgn}(\Delta)}{2}\sqrt{\Delta^2 + \Omega^2} - \left(\bar{E} - \frac{\delta E}{2}\right)\right]dt, \tag{D14}$$

where $\mathrm{sgn}(\Delta)$ means take the sign of Δ. The first line is the adiabatic energy of $\phi_{1,i}$, the first term on the second line is the adiabatic energy when $\delta E = 0$, and the term in parenthesis on the second line is $E(k_i)$. Taylor series expanding Eq. (D14) to first order in δE gives

$$\alpha = \frac{\delta E}{\hbar}\left(\frac{1}{2}\int_{-\infty}^{\infty} -\frac{|\Delta|}{\sqrt{\Delta^2 + \hbar^2\Omega^2(t)}} + 1 dt\right) \equiv \frac{\delta E\ \tau_a}{\hbar}, \tag{D15}$$

where the term in parenthesis can be identified as the time τ_a. By finding the time dependent eigenstates, the term in parenthesis is the integral of the probability to be in the Rydberg state for $\delta E = 0$:

$$\tau_a = \int_{-\infty}^{\infty} \frac{\langle\phi_{R,i}(t)|\phi_{R,i}(t)\rangle|_{\delta E=0}}{\langle\phi_{1,i}(-\infty)|\phi_{1,i}(-\infty)\rangle} dt. \tag{D16}$$

This leads to a $\mathcal{K}_{11}^{(ad)}$ with the same form as Eq. (D3) which implies the χ also has the same form with the parameters as defined below Eq. (D4). The interpretation is the same as below Eq. (D4) and has the same type of scaling. As in the previous sections, if the phase is corrected this gives a value

$$\varepsilon^{(ad)}(\tau_a) = \left(\frac{\delta x}{2\Delta x}\right)^2 = \frac{K^2\tau_a^2 k_B T_{\mathrm{eff}}}{2M}, \tag{D17}$$

where τ_a is defined in Eq. (D16).

For the gate parameters in Table I, we numerically found that Eq. (D17) accurately reproduced the results of the full one atom simulations that included vibrational states.

4. STIRAP pulses

Another method for exciting the Rydberg state is to use stimulated Raman adiabatic passage (STIRAP). This involves two photon excitation with an intermediate state. The two laser pulses only partially overlap and the ordering of the pulses is typically counterintuitive with the laser coupling the intermediate state to the Rydberg state coming before the laser coupling the intermediate state to $|1\rangle$. In this case, it is not obvious how the timing of the pulses will affect the momentum kick to the atom.

To understand this case, we will introduce another state $|p\rangle$ to represent the intermediate state. The Eq. (B3) is modified to

$$\begin{aligned}
i\hbar\frac{\partial\phi_{1,i}(t)}{\partial t} &= [E(k_i) + \hbar\Delta_1]\phi_{1,i}(t) + \frac{\hbar\Omega_1(t)}{2}\phi_{p,i}(t),\\
i\hbar\frac{\partial\phi_{p,i}(t)}{\partial t} &= E(k_i + K_1)\phi_{p,i}(t) + \frac{\hbar\Omega_1(t)}{2}\phi_{1,i}(t) + \frac{\hbar\Omega_R(t)}{2}\phi_{R,i}(t),\\
i\hbar\frac{\partial\phi_{R,i}(t)}{\partial t} &= [E(k_i + K_1 - K_R) - \hbar\Delta_R]\phi_{R,i}(t) + \frac{\hbar\Omega_R(t)}{2}\phi_{p,i}(t),
\end{aligned} \tag{D18}$$

where K_j is the wave number of the photon, Δ_j is the detuning, and Ω_j is the laser coupling of the intermediate state to the states $|j\rangle = |1\rangle$ or $|R\rangle$. Note the - sign for Δ_R is because the Rydberg state is at higher energy than the intermediate state.

In typical STIRAP, the detunings Δ are chosen so that states $|1\rangle$ and $|R\rangle$ are degenerate. If the net recoil is zero $K_1 = K_R$, then this leads to the same equations as when recoil is *not* taken into account. This is because the dark state only involves ϕ_1 and ϕ_R. Thus, there is no decoherence due to recoil when equal frequency photons are used in STIRAP.

If STIRAP is used to excite the Rydberg state and then de-excite it, then this leads to a $\mathcal{K}_{11}^{(S)}$ with the same form as Eq. (D3), which means the χ also has the same form with the parameters as defined below Eq. (D4). The interpretation is the same as below Eq. (D4) and has the same type of scaling. As in the previous sections, if the phase is corrected this gives a value

$$\varepsilon^{(S)} = \left(\frac{\delta x}{2\Delta x}\right)^2 \tag{D19}$$

with the same scaling as previously discussed. The τ is still defined as in Eq. (D16) but the $\delta x = \hbar(K_1 - K_R)\tau/M$.

APPENDIX E: HARMONIC TRAPPING, $V_{\mathrm{tr}} \neq 0$

The case where the trapping potential is on during the gate manipulations can not be solved in the general case. However, the case discussed in Sec. D 2 can be solved for analytically when the atom starts in the motional ground state and can be done analytically for small ε when the atom is in a thermal distribution. We will only present the derivation for the thermal distribution but will give the exact result for the ground state at the end of this section.

Because the duration of each photon pulse is assumed to be much smaller than the oscillation period, the projection is given by

$$\chi^{(HO)} = \sum_{n=0}^{\infty} P_n \langle\psi_n| \left(e^{-iH\tau/\hbar}\right)^{\dagger} e^{-iKx} e^{-iH\tau/\hbar} e^{iKx} |\psi_n\rangle, \quad \text{(E1)}$$

where $P_n = \exp(-\hbar\omega n/[k_B T])/Z$ and $\sum_n P_n = 1$ defines Z. Going from right to left, the operators inside the expectation value come from the photon kick, propagating the result for time τ, the photon kick in the opposite direction, and the time propagation of the $\langle\psi_n|$. If ε is small, then the terms with K can be Taylor series expanded to give

$$\begin{aligned}\langle\psi_n|...|\psi_n\rangle &= 1 - K^2\langle\psi_n|x^2 - e^{iE_n\tau/\hbar} x e^{-iH\tau/\hbar} x|\psi_n\rangle \\ &= 1 - \frac{\hbar K^2}{M\omega}\left[(1-\cos\omega\tau)\left(n+\frac{1}{2}\right) + \frac{i}{2}\sin\omega\tau\right]\end{aligned} \quad \text{(E2)}$$

where the terms linear in x give 0 and we used raising and lowering operators to obtain the second line. The sum over n can be done analytically and gives

$$\chi^{(HO)} = 1 - i\frac{\hbar K^2}{2M\omega}\sin\omega\tau - \frac{K^2 k_B T_{\text{eff}}}{M\omega^2}(1-\cos\omega\tau), \quad \text{(E3)}$$

where T_{eff} is given in Eq. (C7). When evaluating the $|\chi|$, the imaginary term is proportional to K^4 and should be dropped because we are only keeping to order K^2. This gives

$$\varepsilon^{(HO)} = \frac{K^2 k_B T_{\text{eff}}}{M\omega^2}(1-\cos\omega\tau), \quad \text{(E4)}$$

where τ is the time between the pulses. By Taylor series expanding the cosine, Eq. (D11) is obtained. More importantly, it shows that the fractional error in Eq. (D11) is $(\omega\tau)^2/12$ and gives numerical meaning to whether the gate is fast compared to the trapping period. Note that having τ equal to a period of the trap frequency gives $\varepsilon^{(HO)} = 0$.

For the case where there are two very short kicks separated in time by τ, the ground state projection for a harmonic oscillator of angular frequency ω can be found analytically:

$$|\chi|^{(HO,v=0)} = \exp\left[-\frac{\hbar^2 K^2}{2M\hbar\omega}(1-\cos\omega\tau)\right]. \quad \text{(E5)}$$

This result matches that in Eq. (E3) by Taylor series expanding the exponential and noting that $k_B T_{\text{eff}} = \hbar\omega/2$ for $T = 0$.

APPENDIX F: LASER FOCUSING

This section contains effects that arise from the phase and intensity variation for a Gaussian beam. As pointed out in Ref. [46], the intensity dependence of a focused laser can lead to gate infidelity. In addition, there is also phase variation that will be shown to be negligible. To be consistent with the discussion in the other sections, the light propagates in the x direction and the focused beam intensity varies in y and z. In this section, we will also consider the possibility that the focus is not at the origin but at $x = x_0$, $y = y_0$, z where x_0 is an axial misalignment and y_0 is a transverse misalignment. We will assume that both the misalignments and spatial extent of the atomic density distribution are small compared to the waist. If this limit is not satisfied, then the infidelity will be large.

The phase variation has a linear term from the Gouy phase that decreases the momentum kick along the beam axis $K \to K - 1/x_R$ where $x_R = \pi w_0^2/\lambda$ is the Rayleigh range with w_0 the waist. Typically, $Kx_R \gg 10$ so the relative change in the axial momentum can be ignored. In each counter propagating Gaussian beam, there is also a spatially cubic term in the phase

$$\Delta\Phi = \pm\left(\frac{x^3}{3x_R^3} + \frac{x[(y-y_0)^2+z^2]}{x_R w_0^2}\right), \quad \text{(F1)}$$

where the $\pm$ is $+$ for right propagating and $-$ for left propagating, w_0 is the waist, the first term is from the Gouy phase, and the second term is from the curvature of phase fronts. If the excitation is by two photons, the effect from the phase will partially cancel due to the change in sign of the two beams. To estimate the size of the effect from phase variation, we will use a 2 μm waist and note that the spatial extent for 5 μK Cs in a 20 kHz trap is 140 nm. To obtain an idea of the importance, we compare to the phase accumulated by a plane wave Kx. The term from the Gouy phase has a relative contribution of $\sim 10^{-6}$ (for 459 nm) and $\sim 10^{-7}$ (for 1038 nm). The term from the phase front curvature has a relative contribution of $\sim 3\times 10^{-5}$ for each. Thus this effect might be worth revisiting if infidelities less than 10^{-4} become important. Since the extent of the atom density distribution scales like the square root of the temperature, if the temperature were 15 μK, the relative contribution would be 3$\times$ larger.

The focusing leads to a spatial dependence to the electric field strength

$$\begin{aligned}E(x,y,z) &= E_0[1-\eta(x,y,z)], \\ \eta &\equiv \frac{(x-x_0)^2}{2x_R^2} + \frac{(y-y_0)^2+z^2}{w_0^2},\end{aligned} \quad \text{(F2)}$$

where x_R is the Rayleigh range and w_0 is the waist for single photon excitation. For two photon excitation, $1/x_R^2$ is the sum of the squares of the inverse Rayleigh ranges and $1/w_0^2$ is the sum of the squares of the inverse waists. As discussed in Ref. [46] and the supplemental material of Ref. [11], this spatial dependence leads to infidelity.

We will briefly repeat the derivation leading to infidelity for the π-2π-π gate. We will assume that the individual pulses are fast enough to ignore the spatial evolution during a pulse. After a net 2π pulse with fractional error $1-\eta$, the spatial wave function for the $|1\rangle$ state is

$$\psi_{f,1} = \cos[\pi(1-\eta)]\psi_{in,1} \simeq -\left(1 - \frac{\pi^2\eta^2}{2}\right)\psi_{\text{in},1}, \quad \text{(F3)}$$

which leads to

$$\varepsilon^{(G)} = \frac{\pi^2}{2}\langle\eta^2\rangle. \quad \text{(F4)}$$

For typical parameters $w_0 \ll x_R$ but the trapping potential is often substantially weaker in the axial direction so we will keep all the terms. We will assume the temperature is the same along the x, y, and z coordinates and that the trap frequency

is the same in the y and z directions. For this case,

$$\varepsilon^{(G)} = \frac{\pi^2}{2}\left[\frac{3\langle x^2\rangle^2 + 6\langle x^2\rangle x_0^2 + x_0^4}{4x_R^4} + \frac{\left(\langle x^2\rangle + x_0^2\right)\left(2\langle y^2\rangle + y_0^2\right)}{x_R^2 w_0^2} + \frac{8\langle y^2\rangle^2 + 8\langle y^2\rangle y_0^2 + y_0^4}{w_0^4}\right] \tag{F5}$$

where we have used $\langle y^2\rangle = \langle z^2\rangle = k_B T_{\mathrm{eff},\perp}/(M\omega_\perp^2)$, $\langle y^4\rangle = \langle z^4\rangle = 3\langle y^2\rangle^2$, and $\langle x^2\rangle = k_B T_{\mathrm{eff},\parallel}/(M\omega_\parallel^2)$ where the symbols are meant to indicate that the T_{eff} and ω are different for x and y, z.

This is a complicated expression so it is worthwhile to note that in many cases the effect on the axial motion from focusing (first two lines) will be substantially smaller than that from the transverse focusing (last line). In this case, the expression

$$\varepsilon^{(G)} \simeq \frac{\pi^2}{2}\left(\frac{y_0}{w_0}\right)^4 + 4\pi^2\left(\frac{y_0}{w_0}\right)^2\mathcal{D} + 4\pi^2\mathcal{D}^2 \tag{F6}$$

with $\mathcal{D} = k_B T_{\mathrm{eff},\perp}/(M\omega_\perp^2 w_0^2)$ gives a good approximation of the effect from focusing and makes clearer the dependence on parameters.

There is one tricky aspect that arises for the π-2π-π gate. The state $|11\rangle$ has nontrivial time evolution. The first π pulse puts this state into a superposition of $|R1\rangle$ and $|11\rangle$ with most of the population in $|R1\rangle$. The 2π pulse mainly changes the sign of the $|11\rangle$ state. This means the last π pulse rotates almost perfectly opposite the initial π pulse so that the final superposition has $|11\rangle$ to order η^4. Thus, *to the order in this section*, $|11\rangle$ has no decoherence. Only the states $|01\rangle$ and $|10\rangle$ will suffer decoherence from focusing.

[1] M. Saffman, Quantum computing with atomic qubits and Rydberg interactions: Progress and challenges, J. Phys. B **49**, 202001 (2016).

[2] D. Barredo, S. de Leséléuc, V. Lienhard, T. Lahaye, and A. Browaeys, An atom-by-atom assembler of defect-free arbitrary two-dimensional atomic arrays, Science **354**, 1021 (2016).

[3] M. Endres, H. Bernien, A. Keesling, H. Levine, E. R. Anschuetz, A. Krajenbrink, C. Senko, V. Vuletic, M. Greiner, and M. D. Lukin, Atom-by-atom assembly of defect-free one-dimensional cold atom arrays, Science **354**, 1024 (2016).

[4] A. Kumar, T.-Y. Wu, F. Giraldo, and D. S. Weiss, Sorting ultracold atoms in a three-dimensional optical lattice in a realization of Maxwell's demon, Nature (London) **561**, 83 (2018).

[5] D. Ohl de Mello, D. Schäffner, J. Werkmann, T. Preuschoff, L. Kohfahl, M. Schlosser, and G. Birkl, Defect-Free Assembly of 2D Clusters of More than 100 Single-Atom Quantum Systems, Phys. Rev. Lett. **122**, 203601 (2019).

[6] M. O. Brown, T. Thiele, C. Kiehl, T.-W. Hsu, and C. A. Regal, Gray-Molasses Optical-Tweezer Loading: Controlling Collisions for Scaling Atom-Array Assembly, Phys. Rev. X **9**, 011057 (2019).

[7] H. Kim, M. Kim, W. Lee, and J. Ahn, Gerchberg-Saxton algorithm for fast and efficient atom rearrangement in optical tweezer traps, Opt. Express **27**, 2184 (2019).

[8] T. Xia, M. Lichtman, K. Maller, A. W. Carr, M. J. Piotrowicz, L. Isenhower, and M. Saffman, Randomized Benchmarking of Single-Qubit Gates in a 2D Array of Neutral-Atom Qubits, Phys. Rev. Lett. **114**, 100503 (2015).

[9] Y. Wang, A. Kumar, T.-Y. Wu, and D. S. Weiss, Single-qubit gates based on targeted phase shifts in a 3D neutral atom array, Science **352**, 1562 (2016).

[10] C. Sheng, X. He, P. Xu, R. Guo, K. Wang, Z. Xiong, M. Liu, J. Wang, and M. Zhan, High-Fidelity Single-Qubit Gates on Neutral Atoms in a Two-Dimensional Magic-Intensity Optical Dipole Trap Array, Phys. Rev. Lett. **121**, 240501 (2018).

[11] T. M. Graham, M. Kwon, B. Grinkemeyer, A. Marra, X. Jiang, M. Lichtman, Y. Sun, M. Ebert, and M. Saffman, Rydberg Mediated Entanglement in a Two-Dimensional Neutral Atom Qubit Array, Phys. Rev. Lett. **123**, 230501 (2019).

[12] H. Levine, A. Keesling, G. Semeghini, A. Omran, T. T. Wang, S. Ebadi, H. Bernien, M. Greiner, V. Vuletić, H. Pichler, and M. D. Lukin, Parallel Implementation of High-Fidelity Multiqubit Gates with Neutral Atoms, Phys. Rev. Lett. **123**, 170503 (2019).

[13] I. S. Madjarov, J. P. Covey, A. L. Shaw, J. Choi, A. Kale, A. Cooper, H. Pichler, V. Schkolnik, J. R. Williams, and M. Endres, High-fidelity entanglement and detection of alkaline-earth Rydberg atoms, Nat. Phys. **16**, 857 (2020).

[14] D. Jaksch, J. I. Cirac, P. Zoller, S. L. Rolston, R. Côté, and M. D. Lukin, Fast Quantum Gates for Neutral Atoms, Phys. Rev. Lett. **85**, 2208 (2000).

[15] X. L. Zhang, A. T. Gill, L. Isenhower, T. G. Walker, and M. Saffman, Fidelity of a Rydberg blockade quantum gate from simulated quantum process tomography, Phys. Rev. A **85**, 042310 (2012).

[16] T. Xia, X. L. Zhang, and M. Saffman, Analysis of a controlled phase gate using circular Rydberg states, Phys. Rev. A **88**, 062337 (2013).

[17] M. M. Müller, M. Murphy, S. Montangero, T. Calarco, P. Grangier, and A. Browaeys, Implementation of an experimentally feasible controlled-phase gate on two blockaded Rydberg atoms, Phys. Rev. A **89**, 032334 (2014).

[18] D. D. B. Rao and K. Mølmer, Robust Rydberg-interaction gates with adiabatic passage, Phys. Rev. A **89**, 030301(R) (2014).

[19] T. Keating, R. L. Cook, A. M. Hankin, Y.-Y. Jau, G. W. Biedermann, and I. H. Deutsch, Robust quantum logic in neutral atoms via adiabatic Rydberg dressing, Phys. Rev. A **91**, 012337 (2015).

[20] L. S. Theis, F. Motzoi, F. K. Wilhelm, and M. Saffman, A high fidelity Rydberg blockade entangling gate using shaped, analytic pulses, Phys. Rev. A **94**, 032306 (2016).

[21] D. Petrosyan, F. Motzoi, M. Saffman, and K. Mølmer, High-fidelity Rydberg quantum gate via a two-atom dark state, Phys. Rev. A **96**, 042306 (2017).

[22] R. Han, H. K. Ng, and B.-G. Englert, Implementing a neutral-atom controlled-phase gate with a single-Rydberg pulse, Europhys. Lett. **113**, 40001 (2016).

[23] S.-L. Su, E. Liang, S. Zhang, J.-J. Wen, L.-L. Sun, Z. Jin, and A.-D. Zhu, One-step implementation of the Rydberg-Rydberg-interaction gate, Phys. Rev. A **93**, 012306 (2016).

[24] X.-F. Shi and T. A. B. Kennedy, Annulled van der Waals interaction and fast Rydberg quantum gates, Phys. Rev. A **95**, 043429 (2017).

[25] A. Mitra, M. J. Martin, G. W. Biedermann, A. M. Marino, P. M. Poggi, and I. H. Deutsch, Robust Mølmer-Sørensen gate for neutral atoms using rapid adiabatic Rydberg dressing, Phys. Rev. A **101**, 030301 (2020).

[26] M. Saffman, I. I. Beterov, A. Dalal, E. J. Paez, and B. C. Sanders, Symmetric Rydberg controlled$-Z$ gates with adiabatic pulses, Phys. Rev. A **101**, 062309 (2020).

[27] D. Petrosyan, M. Saffman, and K. Mølmer, Grover search algorithm with Rydberg-blockaded atoms: Quantum Monte-Carlo simulations, J. Phys. B: At. Mol. Opt. Phys. **49**, 094004 (2016).

[28] M. Saffman and T. G. Walker, Analysis of a quantum logic device based on dipole-dipole interactions of optically trapped Rydberg atoms, Phys. Rev. A **72**, 022347 (2005).

[29] T. Wilk, A. Gaëtan, C. Evellin, J. Wolters, Y. Miroshnychenko, P. Grangier, and A. Browaeys, Entanglement of Two Individual Neutral Atoms using Rydberg Blockade, Phys. Rev. Lett. **104**, 010502 (2010).

[30] M. A. Nielsen and I. L. Chuang, *Quantum Computation and Quantum Information* (Cambridge University Press, Cambridge, UK, 2000).

[31] M. A. Norcia, A. W. Young, W. J. Eckner, E. Oelker, J. Ye, and A. M. Kaufman, Seconds-scale coherence on an optical clock transition in a tweezer array, Science **366**, 93 (2019).

[32] H. Häffner, C. F. Roos, and R. Blatt, Quantum computing with trapped ions, Phys. Rep. **469**, 155 (2008).

[33] M. Saffman, T. G. Walker, and K. Mølmer, Quantum information with Rydberg atoms, Rev. Mod. Phys. **82**, 2313 (2010).

[34] M. Roghani, H. Helm, and H.-P. Breuer, Entanglement Dynamics of a Strongly Driven Trapped Atom, Phys. Rev. Lett. **106**, 040502 (2011).

[35] J. I. Cirac and P. Zoller, Quantum Computations with Cold Trapped Ions, Phys. Rev. Lett. **74**, 4091 (1995).

[36] W. Li, C. Ates, and I. Lesanovsky, Nonadiabatic Motional Effects and Dissipative Blockade for Rydberg Atoms Excited from Optical Lattices or Microtraps, Phys. Rev. Lett. **110**, 213005 (2013).

[37] The textbook C_Z gate is usually written as $C_Z = \mathrm{diag}(1, 1, 1, -1)$. This can be implemented by coupling state $|0\rangle$ to the Rydberg state. We will use Eq. (10) as the definition of C_Z in this paper.

[38] A. W. Carr and M. Saffman, Doubly Magic Optical Trapping for Cs Atom Hyperfine Clock Transitions, Phys. Rev. Lett. **117**, 150801 (2016).

[39] J. Yang, X. He, R. Guo, P. Xu, K. Wang, C. Sheng, M. Liu, J. Wang, A. Derevianko, and M. Zhan, Coherence Preservation of a Single Neutral Atom Qubit Transferred between Magic-Intensity Optical Traps, Phys. Rev. Lett. **117**, 123201 (2016).

[40] C. A. Sackett, D. Kielpinski, B. E. King, C. Langer, V. Meyer, C. J. Myatt, M. Rowe, Q. A. Turchette, W. M. Itano, D. J. Wineland, and C. Monroe, Experimental entanglement of four particles, Nature (London) **404**, 256 (2000).

[41] B. M. Terhal, Quantum error correction for quantum memories, Rev. Mod. Phys. **87**, 307 (2015).

[42] I. I. Beterov, I. I. Ryabtsev, D. B. Tretyakov, and V. M. Entin, Quasiclassical calculations of blackbody-radiation-induced depopulation rates and effective lifetimes of Rydberg nS, nP, and nD alkali-metal atoms with $n \leqslant 80$, Phys. Rev. A **79**, 052504 (2009).

[43] I. I. Beterov, I. I. Ryabtsev, D. B. Tretyakov, and V. M. Entin, Erratum: Quasiclassical calculations of blackbody-radiation-induced depopulation rates and effective lifetimes of Rydberg nS, nP, and nD alkali-metal atoms with $n \leqslant 80$ [Phys. Rev. A **79**, 052504 (2009)], Phys. Rev. A **80**, 059902(E) (2009).

[44] S. Zhang, F. Robicheaux, and M. Saffman, Magic-wavelength optical traps for Rydberg atoms, Phys. Rev. A **84**, 043408 (2011).

[45] T. G. Walker and M. Saffman, Consequences of Zeeman degeneracy for the van der Waals blockade between Rydberg atoms, Phys. Rev. A **77**, 032723 (2008).

[46] K. Gillen-Christandl, G. Gillen, M. J. Piotrowicz, and M. Saffman, Comparison of Gaussian and super Gaussian laser beams for addressing atomic qubits, Appl. Phys. B **122**, 131 (2016).